U.S. DEPARTMENT OF ENERGY

PNNL-17852

Prepared for the U.S. Department of Energy
Under Contract DE-AC05-76RL01830

Influence of Manufacturing Processes on the Performance of Phantom Lungs

RJ Traub

September 2008

Pacific Northwest
NATIONAL LABORATORY

DISCLAIMER

PACIFIC NORTHWEST NATIONAL LABORATORY
operated by
BATTELLE
for the
UNITED STATES DEPARTMENT OF ENERGY
under Contract DE-AC05-76RL01830

Printed in the United States of America

Available to DOE and DOE contractors from the
Office of Scientific and Technical Information,
P.O. Box 62, Oak Ridge, TN 37831-0062;
ph: (865) 576-8401
fax: (865) 576-5728
email: reports@adonis.osti.gov

Available to the public from the National Technical Information Service,
U.S. Department of Commerce, 5285 Port Royal Rd., Springfield, VA 22161
ph: (800) 553-6847
fax: (703) 605-6900
email: orders@ntis.fedworld.gov
online ordering: http://www.ntis.gov/ordering.htm


This document was printed on recycled paper.
(9/2003)

PNNL17852

Influence of Manufacturing Processes on the Performance of Phantom Lungs

RJ Traub

September 2008

Prepared for
the U.S. Department of Energy
under Contract DE-AC05-76RL01830

Pacific Northwest National Laboratory
Richland, Washington 99352

Executive Summary

The Pacific Northwest National Laboratory (PNNL) operates the U.S. Department of Energy (DOE) Phantom Library that loans phantoms to in vivo bioassay facilities so that they can calibrate their counting systems. A large fraction of the loans request phantom lungs that are inserted into a torso phantom that was designed at the Lawrence Livermore National Laboratory (LLNL). PNNL also manufactures phantom lungs for in vivo counting facilities as well as the DOE Laboratory Accreditation Program accreditation laboratory.

Phantom lungs are made from lung tissue substitutes whose constituents are foaming plastics and various adjuvants selected to make the lung tissue substitute similar to normal healthy lung tissue. The ultimate purpose of the data obtained from these phantom lungs is to assist Health Physicists estimate radiation doses to workers who have inhaled radioactive materials. For this reason, there is considerable interest in ensuring that the stated activity in the phantom lungs is correct.

It is also necessary that phantom lungs have radiological properties identical to those of the human lungs they are designed to emulate. That is, if two sets of phantom lungs containing the identical quantity of radioactive material are placed in the LLNL torso phantom (one set made from human tissue and the other from a lung tissue substitute) and an in vivo bioassay is performed, the person performing the bioassay procedure should not be able to reliably tell which lung set is which. If it is not possible to distinguish between the two sets of lungs, then either set can be used in place of the other.

In this report, the concept of “apparent brightness” is introduced as a metric for the performance of phantom lungs. Apparent brightness refers to the number of photons detected by a chest-counting system per photon emitted in a phantom lung. The term "apparent" is used to indicate that only a fraction of the total photon emission from the phantom lungs is measured. If two sets of phantom lungs have the same apparent brightness, then the two sets of lungs can be used interchangeably because they meet the test previously described.

This report describes several manufacturing processes that can influence the performance of phantom lungs. In some cases, it is possible to quantify and compensate for the influence of the manufacturing processes on the performance of the phantom lungs. In other cases, however, it is possible to only show that an influence exists and to estimate its magnitude.

The manufacturing-related processes investigated for this report were shrinkage of the phantom lungs during curing, skin formation on the surface of the phantom lung, coating the phantom lung with a sealant, variations in density, and the addition of adjuvants to adjust the radiation attenuation properties of the phantom lung.

The influence of some of these manufacturing processes may be inherently unknowable. For example, consider the influence of skin formation. A foaming material is either self-skinning or it is not. The only way to determine the influence of the skin formation process would be to make phantom lungs of self-skinning material and a non self-skinning material and measure the differences. But the inherent variability caused by confounders such as variations in density, elemental composition, activity present in the lung would likely make it impossible to isolate the influence due to the skin.

The influence of other processes such as the protective coating could be measured by counting the phantom lungs in the LLNL torso phantom before and after the sealant had been applied. The calculations presented in this report indicate that the coating may decrease the brightness of the phantom lungs by 4-5%. But even this magnitude of variation may be too small to be reliably detected and quantified by in vivo bioassay equipment.

This work also showed that a large number of lung tissue substitutes can be used to manufacture phantom lungs and still achieve a performance identical to a reference lung material. The single most important metric appears to be the linear attenuation coefficient of the phantom lung tissue substitute. If the linear attenuation coefficients of two lung tissue substitutes are identical, then it appears that the performance of phantom lungs made from those two materials, as quantified by their relative apparent brightness, will also be identical.

Acknowledgments

The author would like to thank Robert Loesch and Steve Zobel of the Department of Energy for their generous support of this work. Thanks also to Tim Lynch of the Pacific Northwest National Laboratory for many fruitful discussions concerning the chest counting systems at the PNNL In Vivo Radiobioassay and Research Facility that formed the basis for the virtual chest counting system described in this report. Dave Payson edited the report and shepherded it through the publication process.

Contents

Figures

Tables

1.0 Introduction

Chest counting is an important tool for estimating the radiation dose to individuals who have inhaled radioactive materials. Standards organizations (DOE 1998; HPS 1996; ISO 2001) have established performance criteria for in vivo measurement laboratories that provide chest-counting services. For chest-counting systems, five measurement categories have been defined that can be used to evaluate the performance of measurement laboratories. Table 1.1 shows the in vivo chest-counting testing categories, the radionuclides included in each category, and the photon energies that would be used to quantify the radionuclides in each category. The photon energies that are used for quantification are seen to range over nearly two orders of magnitude.

Table 1.1. In Vivo Testing Chest-Counting Categories and Photon Energies Used to Quantify the Radionuclides in Each Category[a]

	Measurement Category	Radionuclide	Photon Energy[b,c] (MeV)
I.	Transuranium elements	^{238}Pu	0.01722
	via L x-rays		0.02017
II.	^{241}Am	^{241}Am	0.05954
III.	^{234}Th	^{234}Th in equilibrium with ^{238}U	0.06329
			0.09275
IV.	^{235}U	^{235}U	0.1438
			0.1620
			0.1857
			0.2053
V.	Fission and activation products	Any two of:	0.8348
		^{54}Mn, ^{58}Co, ^{60}Co, or ^{144}Ce	0.511
			0.8108
		Plus:	1.173
		^{134}Cs, ^{137}Cs for interference	1.332
			0.1335
			0.6965
			0.4753
			0.5632
			0.6047
			0.7758
			0.6616

a. HPS 1996; ISO 2001; DOE 1998.

b. Photon energies of the listed radionuclides that are used for bioassay measurements.

c. Energy from ICRP (1983).

In general, the lower-numbered testing categories are more challenging for in vivo measurement laboratories and phantom manufacturing laboratories than are the higher numbered testing categories, because, in general, the lower the number of the testing category the lower the photon energies to be measured. For in vivo measurement laboratories, the lower energy photons are difficult to measure due to anatomical variations in workers, including the thickness and density of the chest wall. For manufacturing laboratories, the attenuation coefficients for lower energy photons are very sensitive to the elemental composition and density of the phantom material, both of which may be difficult to control.

A common approach is to design a phantom organ whose radiological properties, specifically the mass attenuation coefficients at specified photon energies (see Table 1.1), match those of a reference material as closely as possible. Phantom lungs are made from foamed plastics that, like human tissues, contain C, H, O, and N but in different relative amounts. Several types of plastic have been used to manufacture artificial lungs for this phantom (Griffith et al. 1979; Taylor 1997; Traub et al. 2006) and are modified to become more tissue-like by adding adjuvants such as AlOH, Al_2O_3, SiO_2 and $CaCO_3$.

Phantoms are used by in vivo measurement laboratories to calibrate their counting systems and by testing agencies to assess the capabilities of licensee systems. The International Commission on Radiation Units and Measurements (ICRU) (1992a) has published a compendium of phantoms, some of which are used by in vivo measurement laboratories to calibrate their systems. In the United States, the most commonly used phantom for chest-counting systems is that which was developed at the Lawrence Livermore National Laboratory (LLNL) (Griffith et al. 1979). A feature of this phantom is that it provides for interchangeable organs, particularly lungs. A phantom manufacturing laboratory can make phantom organs that contain any desired combination of radionuclides that are used by measurement laboratories to calibrate their chest-counting systems. Testing laboratories distribute phantom organs to test the performance of measurement laboratories against the criteria of the performance standards.

For this report, it was desirable to describe the performance of chest-counting systems as a property of the phantom lung being counted. To achieve this goal, the term "brightness" was borrowed from radiative physics (Weisstein, http://scienceworld.wolfram.com/physics/Brightness.html). In this report, apparent brightness refers to the number of photons detected by a chest-counting system, N_d, per photon emitted, N_e, in a phantom lung. The term "apparent" is used to indicate that only a fraction of the total photon emission from the phantom lungs is measured. The units of apparent brightness are $N_d\, N_e^{-1}$. Because the primary interest is chest-counting systems, the definition of apparent brightness presumes the presence of a phantom that contains the phantom lungs and keeps them in a defined geometry and the presence of radiation detectors that detect a fraction of the radiation emitted from the phantom lungs. Relative apparent brightness is defined to be the apparent brightness of a phantom lung made from any arbitrary material divided by the apparent brightness of a phantom lung made from a reference material. Relative apparent brightness is unitless. Unless otherwise stated the reference lung tissue material is ICRU-44 (ICRU 1989) adult (healthy) lung tissue at a density of 0.26 g cm^{-3} and whose elemental composition is shown in Table 3.1.

2.0 Methods

The phantom and chest-counting system was implemented as input to MCNPX 2.5.e (Hendricks et al. 2004) to calculate the brightness of phantom lungs that had been manufactured in various ways.

2.1 MCNPX Calculations

Numerical experiments were performed using MCNPX version 2.5.e (Hendricks et al. 2004) that were designed to show how the lung tissue substitute used to make the phantom lungs and various manufacturing-related processes will affect the relative apparent brightness of the phantom lungs. Ten photon energies were chosen for these calculations rather than modeling the performance of phantom lungs for a specific radionuclide. The photon energies chosen for this report were selected so that the logs of their energies were about equally spaced between 0.017 MeV and 0.5 MeV. These energies were chosen because this is about the energy range of the chest-counting system that is used at the Pacific Northwest National Laboratory (PNNL) In Vivo Radiobioassay and Research Facility (IVRRF). The photon energies were 0.017, 0.025, 0.036, 0.052, 0.076, 0.111, 0.162, 0.236, 0.343, and 0.5 MeV. The MCNPX source routine was adjusted until the Monte Carlo error associated with the simulated count was nearly the same for all photon energies. This was accomplished by adjusting the source probability for each photon to be proportional to the mass attenuation coefficient of ICRU-44 tissue for that photon energy.

2.1.1 Chest-Counting System

An array of four HPGe detectors, similar to those in use at the IVRRF, was implemented in MCNPX. In the case of the detectors, a single detector was defined, pointing down with the center of the beryllium face located at the origin. This single detector was defined in its own universe, separate from the Norman universe, described below. The detector universe then filled a $2 \times 2 \times 1$ cell hexahedral lattice array which resulted in a four detector array. The detector array was then rotated 90° around its X-axis and translated into position in front of the Norman phantom. Figure 2.1 shows a plan view of the Norman phantom and the HPGe detector array. An elevation view of the Norman phantom and the HPGe array is shown in Figure 2.2.

The photon spectrum in the HPGe detectors was obtained using the "pulse height detector," or f8 tally of MCNPX. This tally reports the total energy deposited in the detector from each incoming photon or electron. For these numerical experiments, the photon energy deposited in the HPGe detectors was partitioned into 4096 channels, each channel being 0.00025 MeV wide.

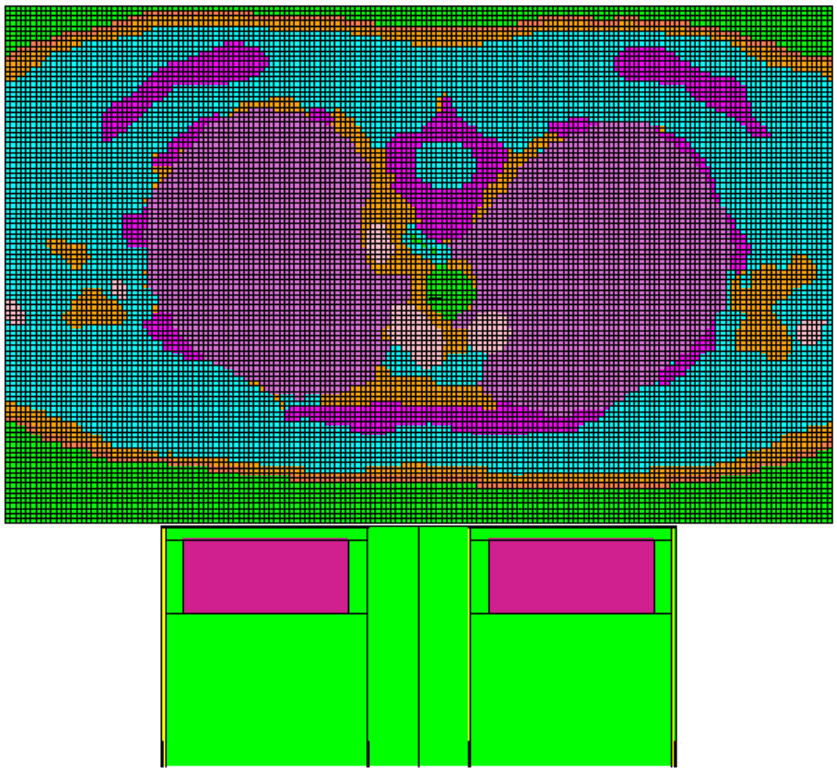

Figure 2.1. Plan View of the Norman Phantom and Two HPGe Detectors

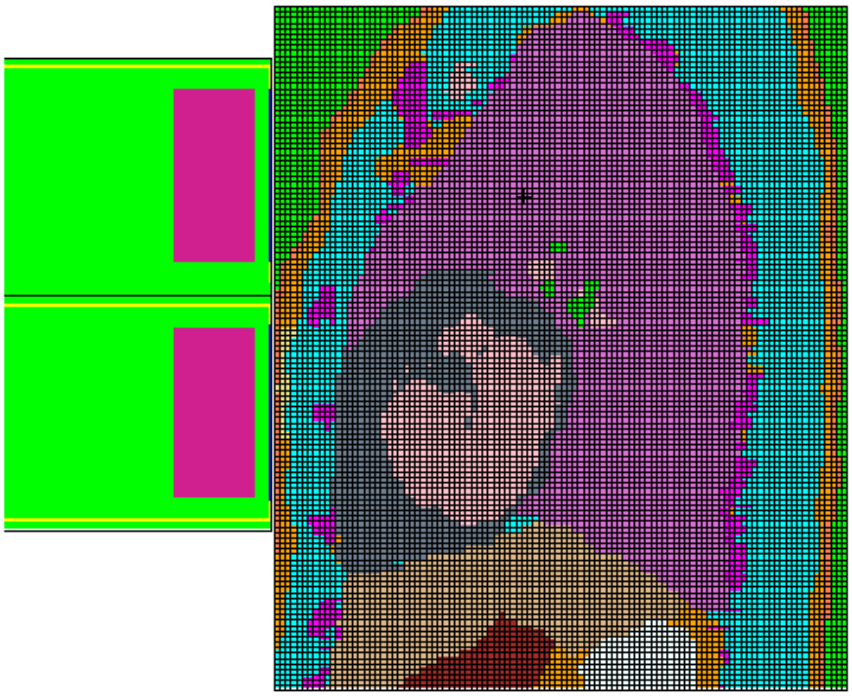

Figure 2.2. Elevation View of the Norman Phantom and Two HPGe Detectors

MCNPX provides a statistical treatment for "pulse height detector" tallies that emulates the Gaussian broadening of peaks due to the statistical nature of the instruments and energy deposition in detectors. The equation used by MCNPX to compute the full width at half maximum of the observed energy broadening in a physical radiation detector (FWHM) is:

$$FWHM = a + b\sqrt{E + cE^2} \tag{2.1}$$

In the above equation, *FWHM* is the full width half maximum of the photopeak, in MeV, *E* is the energy of the incident photon, in MeV, and *a*, *b*, and *c* are constants of the equation. For the calculations reported here, the numerical value of the equations parameters were: *a* = 7.01543e-4, *b* = 1.92241e-4 and *c* = 143.246.

2.2 Phantom

A voxelized description of the Livermore phantom was not available to the author and so the Norman voxel phantom (Dimbylow 1977) was used as a surrogate. The chest region of the Norman phantom was implemented in MCNPX (Hendricks et al. 2004) using the repeated structures capability of MCNPX. The basic unit of the Norman phantom is a voxel with dimensions of 0.2077 cm × 0.2077 cm × 0.2021 cm. The Norman phantom database identifies 38 different tissue types; every voxel in the Norman phantom is defined to be one of those 38 tissue types or air. Each tissue of the Norman phantom was represented as a 1-cm-diameter sphere located at the origin (x=y=z=0.0) of its own universe. Thus the tissues of the Norman phantom consisted of 38 superimposed but unique 1-cm-diameter spherical universes. The tissue universes filled a 163 × 104 × 51 cell hexahedral lattice array.

Each voxel of the Norman phantom was filled with the universe that described its location within the phantom. Thus, for example, the voxels that represented the lung were filled with the lung universe and voxels that represented bone were filled with the bone universe. Each universe had unique density and elemental composition. The elemental composition of the organs and tissues of the Norman phantom was obtained from ICRU publications (ICRU 1984; ICRU 1989; ICRU 1992b).

2.3 Surface of Phantom Lung

For some calculations it was necessary to identify the voxels on the surface of the lungs of the Norman phantom. To identify the surface voxels, a mathematical filter was written in the Matlab® (The MathWorks, Inc., Natick, MA 01760) programming language that would modify the properties of the surface layer of the lung tissue region of the phantom. Briefly, the filter interrogated each voxel of the phantom to determine the tissue type of the voxel as defined by the universe that filled the voxel. If the voxel contained lung tissue, and if any of the 26 voxels that surrounded the voxel of interest did not contain lung tissue, then the universe of the voxel was converted from that of lung tissue to the lung surface material. The mathematical filter counted the total number of lung voxels in the Norman phantom, the number of conversions performed, and the number of lung voxels that were not transformed. There were 465,633 lung voxels in the original Norman phantom, 384,911 lung voxels in interior region of the lung, and 80,722 voxels in the surface region. These data indicate that the lung volume of the Norman phantom is 4.06×10^{-3} m^3, which is less than the ICRP (2002) value of 5.02×10^{-3} m^3 for the vital capacity.

A voxel is the smallest unit of the phantom and can contain only one universe. To simulate a 2-mm layer that actually has multiple layers of different materials and at different densities, a single hybrid material was defined whose elemental composition and density was computed from the volume fractions of the constituent materials.

2.4 Data Analysis

The data generated by MCNPX were written to a MCTAL file, a concise and well-documented data format, and then imported into Excel for analysis. A simple gamma spectrometer was implemented in Excel to obtain the "counts" in the photopeaks of the originating photons. The region of interest (ROI) for each photopeak was determined by inspection of the Excel plots. Background, defined as the average count of the three channels above the ROI and the three channels below the ROI, was subtracted from the gross counts in each channel of the photopeak to obtain a net photopeak count. The relative errors of the Monte Carlo calculations were propagated for all calculations. Although not shown on the plots and tables of this report, the relative errors were less than 1% for all calculations.

The apparent brightness of the phantom lungs was calculated by summing the net counts of a particular incident photon in all four detectors and then dividing that sum by the number of photons emitted in the phantom lung. The relative apparent brightness was calculated by dividing the apparent brightness of a phantom lung made from a test material divided by the apparent brightness of a phantom lung made of ICRU-44 tissue at a density of 0.26 g cm^{-3}.

3.0 Radiological Properties

The radiological properties of 13 lung tissue substitutes were evaluated. The reference lung material was the healthy adult lung tissue listed in ICRU-44 (ICRU 1989) and ICRP-89 (ICRP 2002), referred here as ICRU-44 lung tissue. The lung tissue substitutes investigated included that developed by Griffith (Griffith et al 1979; ICRU 1989) designated Grif-G, a second lung tissue substitute developed at LLNL, designated LLLL1 (Taylor,1997) , ALT2 (Traub et al. 2006), the Alderson Lung material (ICRU 1989), LN1 (Fry and Summerling 1982), LN10/75 (ICRU 1989), MS20/L (Fry and Summerling 1982), LTES (Fry and Summerling 1982), LN300 (Blanchard 2005), and an unnamed material designated here as SK_LNG (Kinase et al. 2005). Two additional tissue substitutes, A150 and M3 (ICRU 1984), were included. The latter two tissue substitutes were included to determine if they would be acceptable substitutes if they could be made at the correct density. The elemental compositions of these tissues and tissue substitutes are listed in Tables 3.1 and 3.2.

Table 3.1. Elemental Compositions of Lung Tissue and Lung Tissue Substitutes

	Lung Tissue Substitute					
	ICRU-44	Grif-G	LLLL1	ALT2	LTES	LN300
	Published Density (g cm^{-3})					
	0.26	0.26	0.28	0.26	0.3	0.3
Element	Weight Fraction					
H	0.103	0.080	0.089	0.0840	0.07	0.08465
C	0.105	0.608	0.667	0.6130	0.574	0.59475
N	0.031	0.042	0.036	0.0322	0.021	0.01965
O	0.749	0.248	0.193	0.2489	0.224	0.18125
F	m	m	m	m	m	m
Na	0.002	m	m	m	m	m
Mg	m	0.001	m	m	0.093	0.112
Al	m	m	m	m	m	m
Si	m	m	m	m	0.017	0.0068
P	0.002	m	m	m	m	m
S	0.003	m	m	m	m	m
Cl	0.003	m	m	0.0004	0.001	0.001
Ar	m	m	m	m	m	m
K	0.002	m	m	m	m	m
Ca		0.021	0.015	0.0211	m	m
Ti	m	m	m	m	m	m
Mn	m	m	m	m	m	m
Fe	m	m	m	m	m	m
Zn	m	m	m	m	m	m
Rb	m	m	m	m	m	m
Sn	m	0.0002	m	m	m	m

m – Element not present in material.

Table 3.2. Elemental Compositions of Lung Tissue Substitutes

	Lung Tissue Substitute						
	M3	A-150	LN1	LN10/75	MS20/L	Aldsn	SK_LNG
	Published Density (g cm^{-3})						
	1.05	1.127	0.25-0.30	0.31	0.25-0.30	0.32	0.24
Element	Weight Fraction						
H	0.114318	0.101327	0.060	0.084	0.0837	0.057	0.0699
C	0.655823	0.775501	0.514	0.604	0.5996	0.740	0.6161
N	m	0.035057	0.043	0.017	0.0199	0.020	0.0631
O	0.092183	0.052316	0.307	0.173	0.1802	0.181	0.2064
F	m	0.017422	m	m	m	m	m
Na	m	m	m	m	m	m	m
Mg	0.134792	m	m	0.114	0.1139	m	m
Al	m	m	0.076	m	m	m	m
Si	m	m	m	0.007	m	m	m
P	m	m	m	m	m	m	0.0100
S	m	m	m	m	m	m	m
Cl	m	m	m	0.001	0.001	m	0.0345
Ar	m	m	m	m	m	m	m
K	m	m	m	m	m	m	m
Ca	0.002883	0.018378	m	m	m	m	m
Ti	m	m	m	m	m	m	m
Mn	m	m	m	m	m	m	m
Fe	m	m	m	m	m	m	m
Zn	m	m	m	m	m	m	m
Rb	m	m	m	m	m	m	m
Sn	m	m	m	m	m	0.002	m

m – Element not present in material.

The radiological properties investigated for these materials were the mean excitation energy, I, the electron density, n_0, the effective atomic number of the material, Z_{eff}, and the photon mass attenuation coefficients. The radiological properties described are commonly requested by PNNL customers even though some of the properties are not strictly associated with the radiation attenuation properties of the lung tissue substitutes.

3.1 Methods

The mean excitation energy I (eV) of each lung tissue substitute was calculated using the Bragg additivity rule, equation (1), using I-values for elemental constituents as shown in Tables 4.3 and 5.1 of (ICRU-37, p. 23).

$$\ln(I) = \left[\sum_j w_j \left(\frac{Z_j}{A_j} \right) \ln(I_j) \right] \left\langle \frac{Z}{A} \right\rangle^{-1} \tag{3.1}$$

where

$$\left\langle \frac{Z}{A} \right\rangle = \sum_j w_j \left(\frac{Z_j}{A_j} \right) \tag{3.2}$$

w_j is the fraction by weight, and Z_j, A_j , and I_j pertain to the atomic number, atomic weight, and excitation energy (eV) of the j'th constituent.

The electron density, n_0, was calculated using equation (3.3):

$$n_0 = \rho N_A \sum_j \frac{w_j Z_j}{A_j} \tag{3.3}$$

where N_A is Avogadro's constant and ρ is the density of the material in g m^{-3}.

The effective atomic number of the material, Z_{eff}, was calculated using equation (3.4): Johns and Cunningham (1977)

$$Z_{eff} = \sqrt[m]{\sum_j a_j Z_j^m} \tag{3.4}$$

where m = 2.94 and a_j is the fractional content of electrons belonging to the j'th constituent.

Photon mass attenuation coefficients, without coherent scattering, were obtained directly from XCOM (Berger et al. 2005), a photon cross-sections database, at the 10 test photon energies.

The apparent brightness of phantom lungs, described above, was calculated for each of the thirteen lung tissues and lung tissue substitutes at the same 10 photon energies chosen for the mass attenuation coefficients.

3.2 Results

The elemental compositions of the lung tissue and lung tissue substitutes are listed in Table 3.1 and Table 3.2. The mean excitation energy, I, the effective atomic number, Z_{eff}, and electron density, n_0, of the thirteen lung tissues and lung tissue substitutes and the total photon mass attenuation coefficients, without coherent scatter, of the human lung tissues and lung tissue substitutes are listed in Table 3.3 for ten experimental photon energies. The apparent brightness and relative apparent brightness, described in the main text of this report, for lung tissue and lung tissue substitutes, are listed in Tables 3.4 and Table 3.5.

Table 3.3. Radiological Properties and Mass Attenuation Coefficients of Lung Tissue and Lung Tissue Substitutes

	ICRU-44	Grif-G	LLLL1	ALT2	LTES	LN300
Density	0.26/1.05	0.26	0.28	0.26	0.3	0.3
n_0	8.62	8.44	8.51	8.47	8.35	8.47
I	75.1	70.9	68.1	70.2	76.2	72.9
Z_{eff}	7.49	7.49	6.97	7.37	7.50	7.39
Photon Energy (MeV)	Mass Attenuation Coefficient – Total Without Coherent Scatter ($cm^2\ g^{-1}$)					
0.017	1.127E+00	1.113E+00	9.455E-01	1.108E+00	1.126E+00	1.099E+00
0.025	4.573E-01	4.612E-01	4.101E-01	4.600E-01	4.557E-01	4.499E-01
0.036	2.668E-01	2.731E-01	2.533E-01	2.689E-01	2.633E-01	2.632E-01
0.052	2.038E-01	2.046E-01	1.992E-01	2.035E-01	1.992E-01	2.009E-01
0.076	1.772E-01	1.754E-01	1.747E-01	1.754E-01	1.723E-01	1.743E-01
0.111	1.598E-01	1.571E-01	1.578E-01	1.575E-01	1.550E-01	1.570E-01
0.162	1.436E-01	1.409E-01	1.419E-01	1.414E-01	1.393E-01	1.411E-01
0.236	1.274E-01	1.248E-01	1.258E-01	1.253E-01	1.235E-01	1.251E-01
0.343	1.113E-01	1.091E-01	1.100E-01	1.095E-01	1.079E-01	1.094E-01
0.500	9.585E-02	9.388E-02	9.465E-02	9.423E-02	9.291E-02	9.415E-02

	M3	A-150	LN1	LN10/75	MS20/L	Aldsn	SK_LNG
Density	1.05	1.127	0.25-0.3	0.31	0.25-0.30	0.32	0.26
n_0	8.69	8.60	8.27	8.46	8.44	8.26	8.36
I	66.9	59.9	78.3	72.9	72.7	72.2	73.1
Z_{eff}	7.32	6.88	7.47	7.40	7.32	7.52	7.51
Photon Energy (MeV)	Mass Attenuation Coefficient – Total Without Coherent Scatter ($cm^2\ g^{-1}$)						
17	1.116E+00	9.368E-01	1.089E+00	1.102E+00	1.064E+00	7.035E-01	1.142E+00
25	4.606E-01	4.114E-01	4.426E-01	4.506E-01	4.389E-01	3.299E-01	4.656E-01
36	2.707E-01	2.559E-01	2.576E-01	2.634E-01	2.596E-01	2.667E-01	2.678E-01
52	2.067E-01	2.015E-01	1.962E-01	2.009E-01	1.997E-01	2.020E-01	2.011E-01
76	1.792E-01	1.767E-01	1.701E-01	1.742E-01	1.739E-01	1.730E-01	1.729E-01
111	1.614E-01	1.595E-01	1.533E-01	1.569E-01	1.568E-01	1.544E-01	1.552E-01
162	1.449E-01	1.434E-01	1.378E-01	1.410E-01	1.410E-01	1.382E-01	1.393E-01
236	1.285E-01	1.271E-01	1.222E-01	1.251E-01	1.250E-01	1.223E-01	1.235E-01
343	1.123E-01	1.111E-01	1.068E-01	1.093E-01	1.093E-01	1.068E-01	1.079E-01
500	9.668E-02	9.562E-02	9.193E-02	9.409E-02	9.408E-02	9.190E-02	9.287E-02

Table 3.4. Apparent Brightness of Lung Tissue and Lung Tissue Substitutes

Photon Energy (MeV)	Apparent Brightness at 0.26 g cm^{-3} $(N_d N_e^{-1})$						
	ICRU-44		Grif-G	LLLL1	ALT2	LTES	LN300
17	3.24E-04		3.29E-04	3.79E-04	3.33E-04	3.22E-04	3.36E-04
25	4.49E-03		4.48E-03	4.73E-03	4.47E-03	4.49E-03	4.52E-03
36	1.05E-02		1.05E-02	1.07E-02	1.06E-02	1.06E-02	1.06E-02
52	1.47E-02		1.48E-02	1.48E-02	1.47E-02	1.49E-02	1.48E-02
76	1.66E-02		1.66E-02	1.66E-02	1.66E-02	1.66E-02	1.66E-02
111	1.71E-02		1.72E-02	1.72E-02	1.72E-02	1.72E-02	1.72E-02
162	1.57E-02		1.57E-02	1.57E-02	1.57E-02	1.57E-02	1.57E-02
236	1.25E-02		1.26E-02	1.26E-02	1.26E-02	1.26E-02	1.26E-02
343	8.95E-03		8.96E-03	8.96E-03	8.95E-03	8.98E-03	8.95E-03
500	4.91E-03		4.93E-03	4.92E-03	4.93E-03	4.93E-03	4.93E-03
Photon Energy (MeV)	Apparent Brightness at 0.26 g cm^{-3} $(N_d N_e^{-1})$						
	M3	A-150	LN1	LN10/75	MS20/L	Aldsn	SK_LNG
17	3.27E-04	3.80E-04	3.32E-04	3.35E-04	3.41E-04	4.77E-04	3.14E-04
25	4.49E-03	4.72E-03	4.55E-03	4.52E-03	4.58E-03	5.37E-03	4.43E-03
36	1.05E-02	1.07E-02	1.06E-02	1.06E-02	1.06E-02	1.06E-02	1.05E-02
52	1.47E-02	1.48E-02	1.49E-02	1.48E-02	1.48E-02	1.48E-02	1.49E-02
76	1.65E-02	1.65E-02	1.68E-02	1.66E-02	1.66E-02	1.67E-02	1.67E-02
111	1.71E-02	1.71E-02	1.73E-02	1.72E-02	1.72E-02	1.72E-02	1.72E-02
162	1.56E-02	1.57E-02	1.57E-02	1.57E-02	1.58E-02	1.58E-02	1.57E-02
236	1.26E-02	1.25E-02	1.26E-02	1.26E-02	1.26E-02	1.26E-02	1.26E-02
343	8.92E-03	8.94E-03	8.98E-03	8.96E-03	8.96E-03	8.99E-03	8.97E-03
500	4.91E-03	4.91E-03	4.94E-03	4.92E-03	4.92E-03	4.94E-03	4.93E-03

Table 3.5. Relative Apparent Brightness of Lung Tissue and Lung Tissue Substitutes

Photon Energy (MeV)	Relative Apparent Brightness at 0.26 g cm^{-3}						
	ICRU-44		Grif-G	LLLL1	ALT2	LTES	LN300
17	1.0000		1.0139	1.1701	1.0289	0.9925	1.0358
25	1.0000		0.9976	1.0537	0.9946	0.9986	1.0066
36	1.0000		0.9923	1.0169	1.0003	1.0074	1.0033
52	1.0000		1.0057	1.0053	0.9998	1.0089	1.0065
76	1.0000		0.9998	1.0031	1.0025	1.0013	1.0041
111	1.0000		1.0058	1.0049	1.0051	1.0055	1.0065
162	1.0000		1.0011	1.0016	1.0011	1.0053	1.0010
236	1.0000		1.0031	1.0006	1.0006	1.0029	1.0038
343	1.0000		1.0010	1.0012	1.0000	1.0030	1.0001
500	1.0000		1.0037	1.0010	1.0038	1.0032	1.0042
Photon Energy (MeV)	Relative Apparent Brightness at 0.26 g cm^{-3}						
	M3	A-150	LN1	LN10/75	MS20/L	Aldsn	SK_LNG
17	1.0093	1.1711	1.0246	1.0324	1.0531	1.4718	0.9688
25	0.9993	1.0499	1.0133	1.0063	1.0193	1.1959	0.9851
36	0.9971	1.0149	1.0094	1.0041	1.0067	1.0029	0.9988
52	1.0007	1.0026	1.0133	1.0053	1.0067	1.0022	1.0115
76	0.9938	0.9982	1.0122	1.0042	1.0044	1.0060	1.0062
111	1.0003	0.9986	1.0125	1.0057	1.0046	1.0087	1.0055
162	0.9952	1.0012	1.0048	1.0028	1.0059	1.0069	1.0034
236	1.0007	0.9984	1.0059	1.0014	1.0013	1.0065	1.0048
343	0.9967	0.9990	1.0035	1.0012	1.0014	1.0051	1.0029
500	0.9984	1.0001	1.0050	1.0020	1.0024	1.0052	1.0041

The relationships between phantom lung brightness and n_0, I, and Z_{eff} for several lung tissue substitutes are shown in Figure 3.1, Figure 3.2, and Figure 3.3, respectively. The lines show little curvature. Because the lines appear almost flat, the brightness of the lungs appears to be independent of the radiological properties investigated. We also investigated if the relative apparent brightness (the apparent brightness of a lung tissue) substitute divided by the apparent brightness of human lung tissue would show any relationship with the radiological properties or the relative values of the radiological properties of those same tissues. The relationships between the relative apparent brightness of the lung tissue substitutes and the relative n_0, I, and Z_{eff} are shown in Figure 3.4, Figure 3.5, and Figure 3.6, respectively.

For some materials there appears to be a partial correlation between relative apparent brightness and photon energy for various radiological properties. This relationship, however, is seen only at low energies; 0.03 MeV and lower.

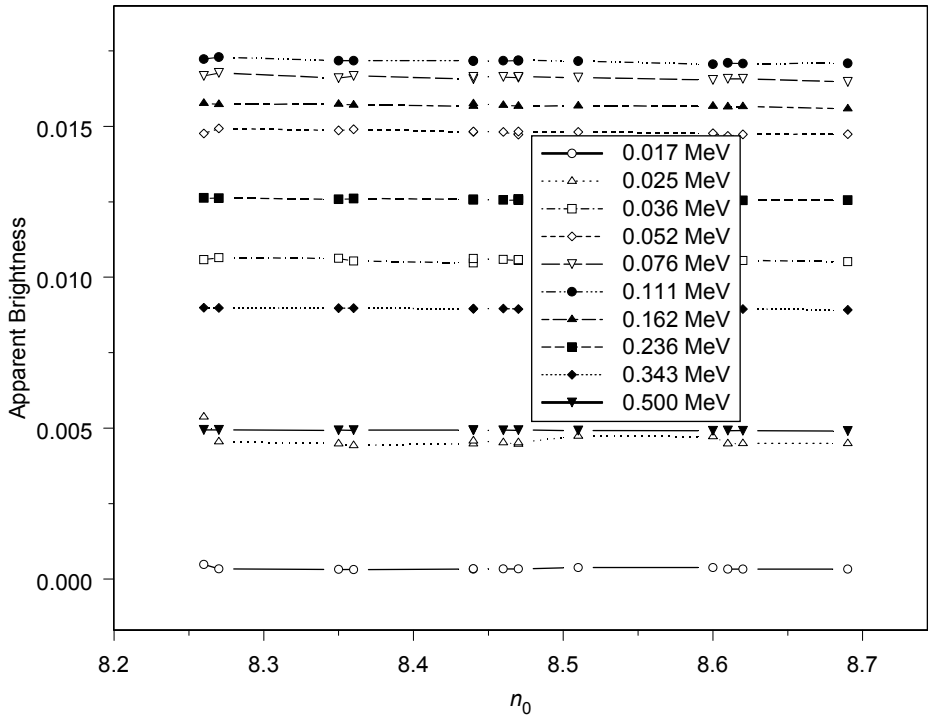

Figure 3.1. Apparent Brightness of Lung Tissue Substitutes as a Function of n_0

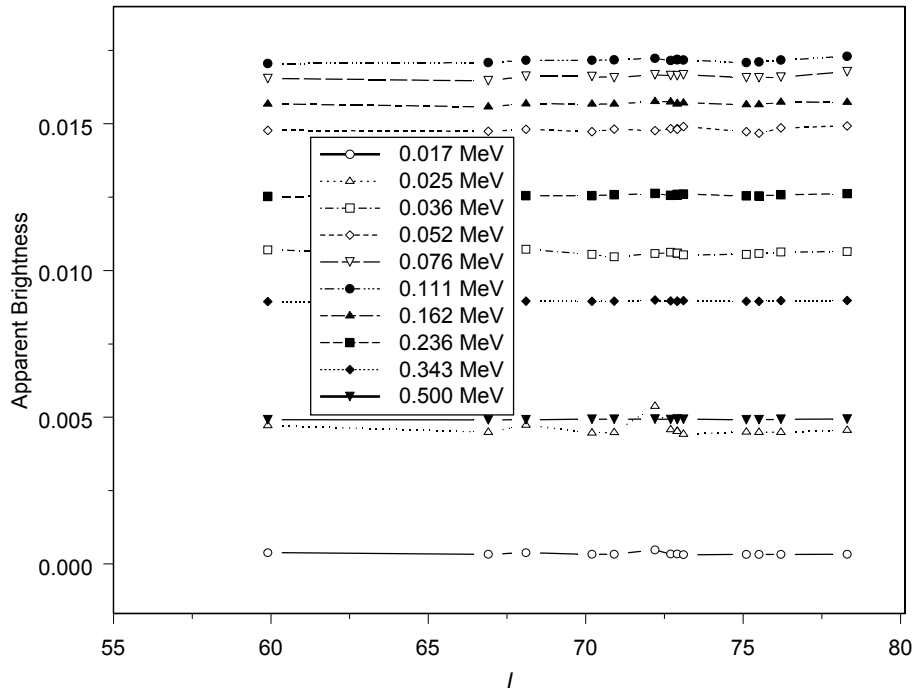

Figure 3.2. Apparent Brightness of Lung Tissue Substitutes as a Function of I

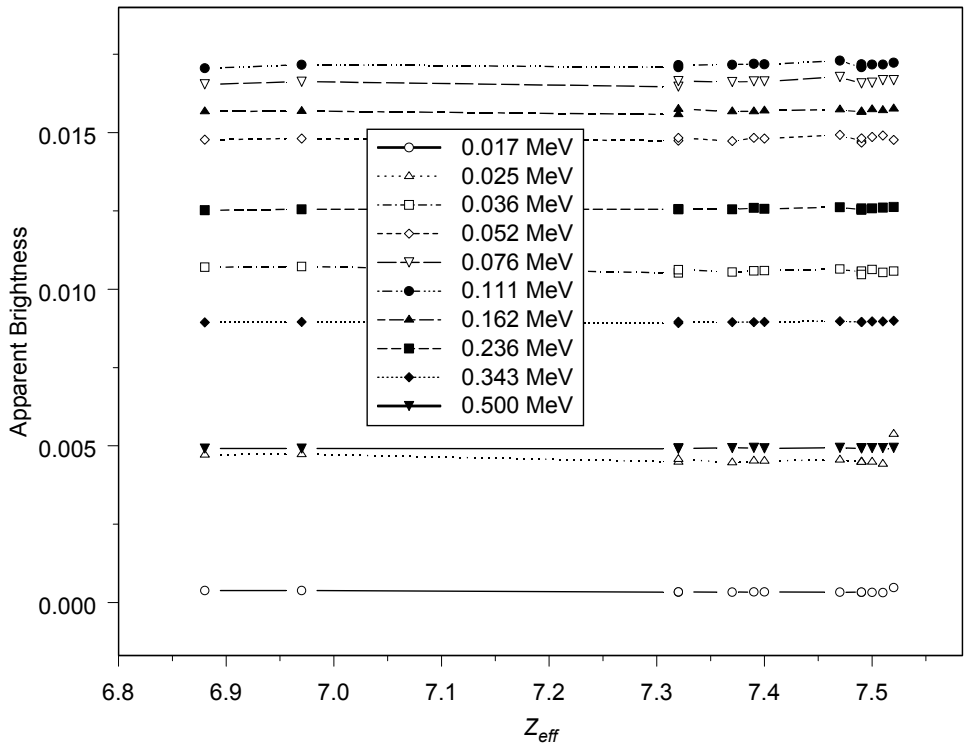

Figure 3.3. Apparent Brightness of Lung Tissue Substitutes as a Function of Z_{eff}

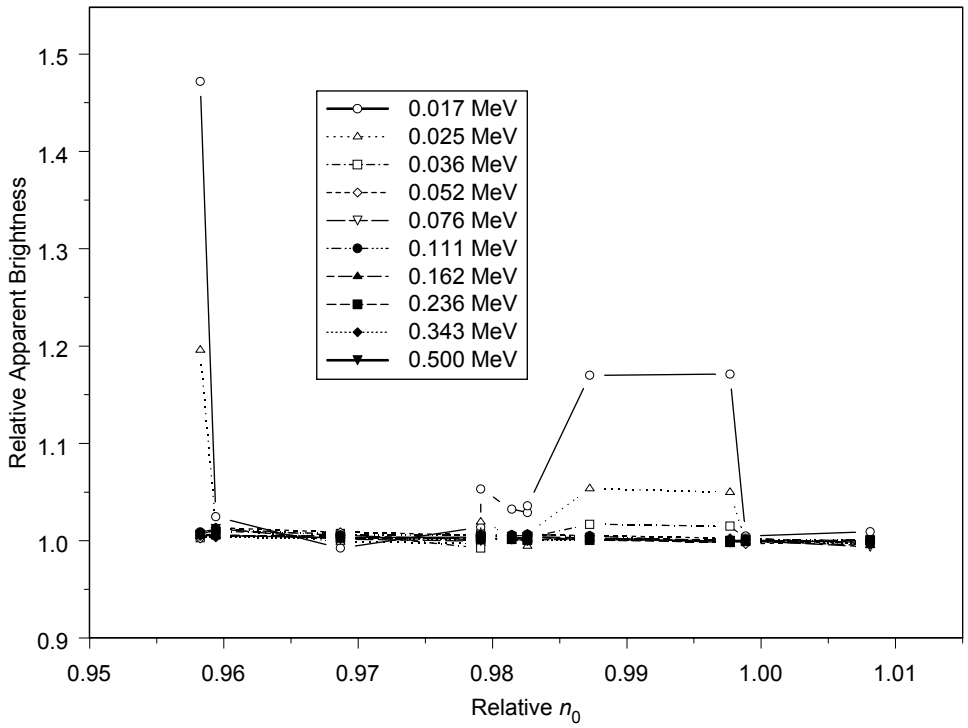

Figure 3.4. Relative Apparent Brightness of Lung Tissue Substitutes as a Function of Relative n_0

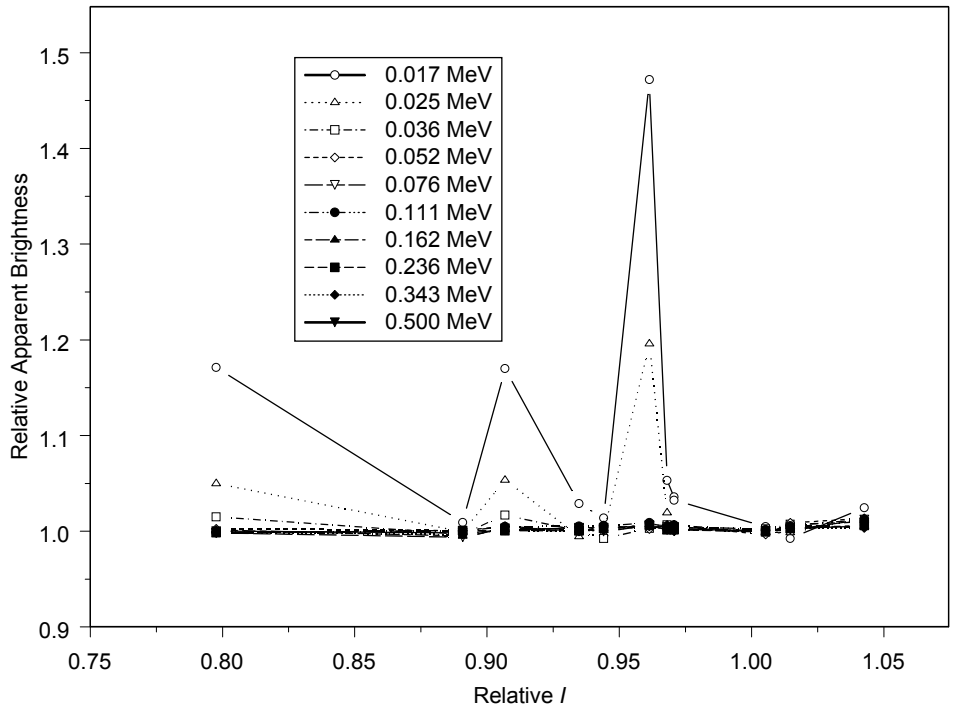

Figure 3.5. Relative Apparent Brightness of Lung Tissue Substitutes as a Function of Relative *I*

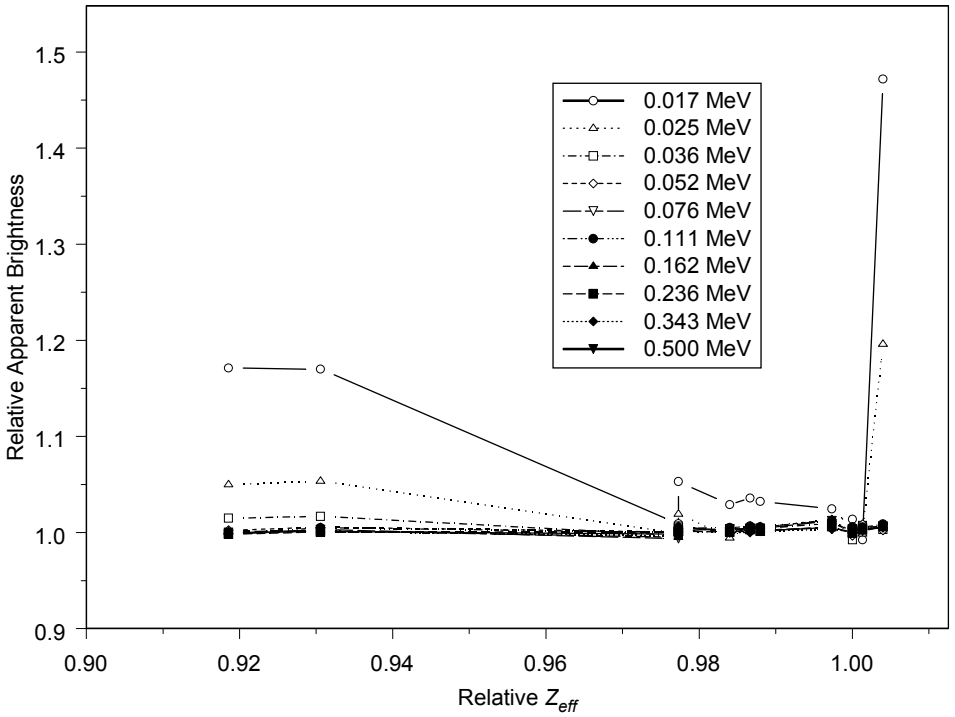

Figure 3.6. Relative Apparent Brightness of Lung Tissue Substitutes as a Function of Relative Z_{eff}

4.0 Density Study

The ease of controlling the density of the phantom lungs depends on many aspects of the manufacturing process, including the design of the lung molds. After phantom lungs have been made, however, the final density of the phantom lungs is readily obtained from the volume of the lungs and their measured mass. A numerical experiment was performed to quantify the influence of phantom lung density on the brightness of phantom lungs. If the density-brightness relationship can be quantified for a particular lung tissue substitute, then it will be possible to normalize the brightness of any given phantom lung to the brightness of a lung made from reference human tissue.

4.1 Methods

MCNPX was used to perform Monte Carlo experiments that used the ALT2 (Traub et al. 2006) lung tissue substitute in the Norman phantom lungs. The density of the ALT2 material was varied from 0.2 to 0.32 g cm^{-3} in 0.02 g cm^{-3} increments.

4.2 Results

Figure 4.1 shows the influence of phantom lung density on the apparent brightness of phantom lungs made of ALT2 lung tissue substitute. The data show an inverse relationship between the density of the phantom lungs and their apparent brightness. The plots are somewhat deceptive in that they seem to indicate that there is a larger change in the brightness of phantom lungs at high photon energies than at low photon energies. While the absolute change is less at low photon energies, the fractional change in brightness is greater for low energy photons.

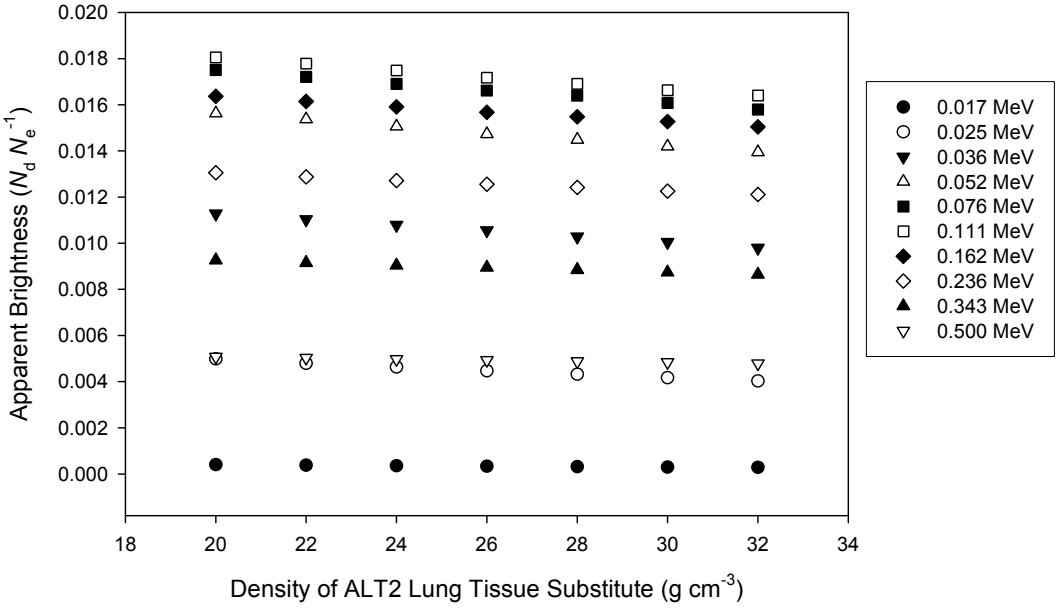

Figure 4.1. Apparent Brightness of ALT2 Phantom Lungs as a Function of Density

Figure 4.2 shows the influence of phantom lung densities on the relative apparent brightness of phantom lungs made from ALT2 lung tissue substitute. The data show that the variation of the brightness of the lung increases as the photon energy decreases. The plots in Figure 4.2 show that the brightness of ALT2 lungs would vary by about 42 % for 0.017-MeV photons when the density ranged from 0.20 to 0.32 g cm^{-3}. Figure 4.3 is a plot of the counting efficiency of the chest-counting system as a function of the photon energy. It can be seen that, for the photon energies included in this study, the maximum apparent brightness is for 0.111 MeV photons. The shape of the curve is because as the photon energy increases, more photons are able to escape from the phantom lungs and enter the radiation detector. Simultaneously, the fraction of photons that enter the detector and deposit all of their energy decreases. At photon energies less than 0.111 MeV the first process predominates while at photon energies greater than 0.111 MeV the second process predominates.

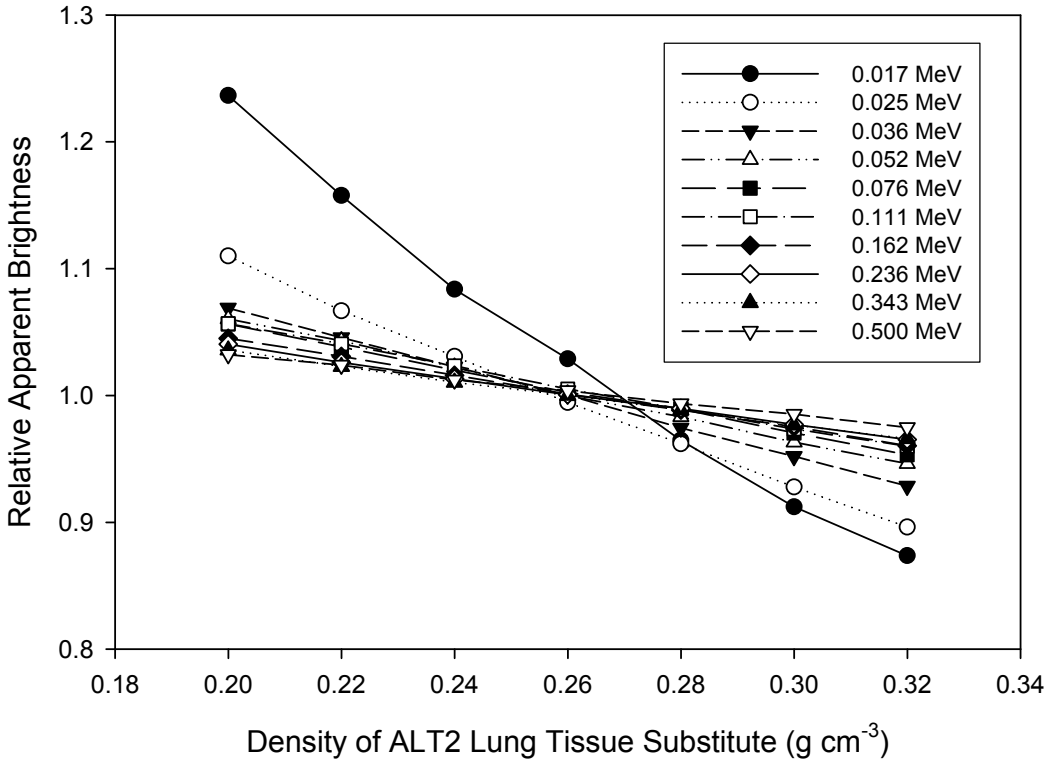

Figure 4.2. Relative Apparent Brightness of Phantom Lungs That Contain ALT2 Lung Tissue Substitute as a Function of the Phantom Lung Density

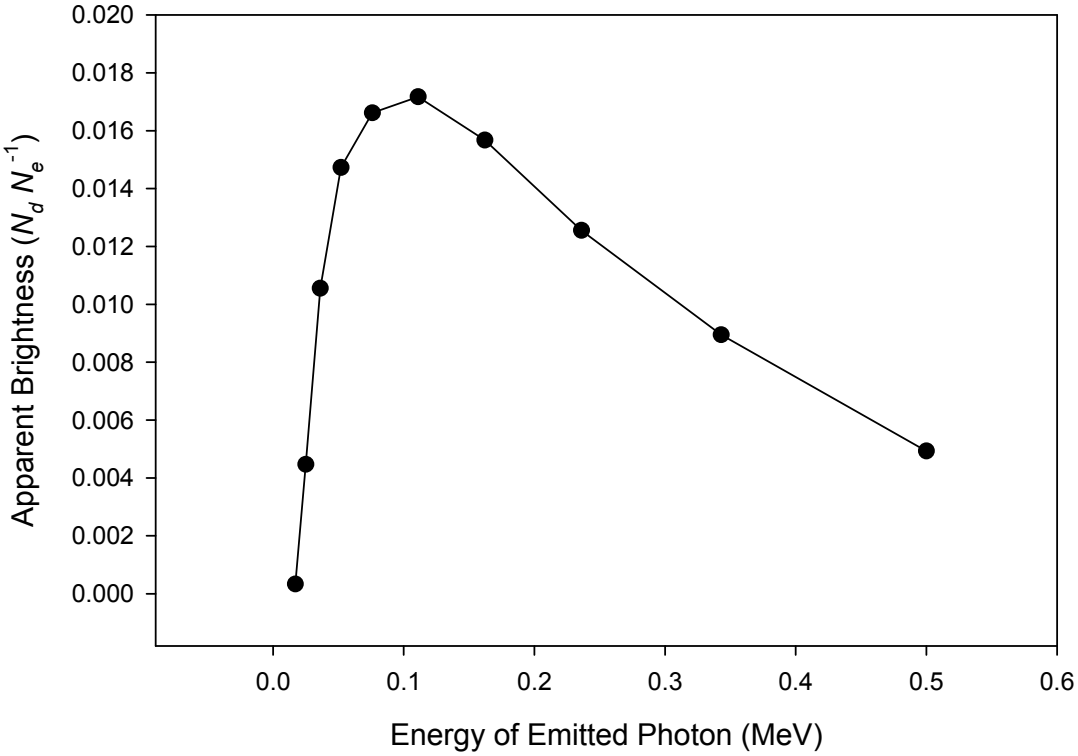

Figure 4.3. Apparent Brightness of ALT2 Phantom Lungs at a density of 0.26 g cm^{-3} as a Function of the Originating Photon Energy

5.0 Shrinkage Study

In some instances, phantom lungs have shrunk shortly after removal from the molds. This numerical experiment was intended to show how shrinkage would affect the brightness of the shrunken phantom lungs. To shrink the lungs of the Norman voxel phantom, the 1-voxel-thick surface layer of the phantom lung was redefined as a new material whose characteristics depended on the amount of shrinkage modeled. The density of the lung tissue substitute in the voxels of the interior region of the phantom lung was increased so that the total mass of the shrunken lung was the same as the mass of the original lung. Identification of the surface voxels was accomplished using the method described in Section 3.3.

5.1 Methods

Two experiments were performed with the shrunken lung. For the first experiment the entire surface region was defined to be air. The width of each voxel is about 2 mm and this experiment assumes that the cross-sectional chord of the lung, in any direction, was reduced by a total of about 4 mm. This shrinkage was greater than has been observed and represents an extreme case of phantom lung shrinkage. The density of the interior lung region was increased by 1.21, relative to the original phantom lung density, to maintain the phantom lung mass. The second experiment assumed slightly less shrinkage of the phantom lung. In this experiment, the surface region was 50% air and 50% lung tissue substitute, by volume. This experiment assumed that the cross-sectional chord, in any direction was reduced by 2 mm. The density of the lung material in the interior region of the lung was increased by a factor of 1.105, relative to the original phantom lung density, to maintain lung mass. Because the phantom lung material was assumed to extend into the transformed region of the phantom lung, the surface region of the phantom lung was defined as lung tissue substitute that was one-half the density of the lung tissue substitute in the interior region of the lung.

For these experiments, it was necessary to modify the source term used by MCNPX so that the simulated radiation was emitted only from the phantom lung material. Because MCNPX was set so that the source was lung tissue, no modifications were necessary for the first experiment. For the second experiment, the phantom lung material in the surface region contained lung material, and thus radioactivity, but at a lower quantity per voxel than was the case for the lung voxels in the interior region of the phantom lung. To account for the two regions where radioactivity could be located, the source definition of MCNPX was adjusted so that, for the one-half voxel reduction case, 91.3% of the photons were emitted from the interior region of the phantom lung and the balance of the photons were emitted from the surface region of the phantom lung to account for the removal of activity from the surface voxels to the interior voxels.

5.2 Results

The results of the lung shrinkage experiments are shown in Table 5.1, and a plot of the data is shown in Figure 5.1. The data presented in Table 5.1 show the anticipated counting efficiency for the photon of the stated energy for the two lung-size-reduction experiments.

Table 5.1. Reduction in the Relative Apparent Brightness of Phantom Lungs due to Shrinkage of the Phantom Lung

	Relative Apparent Brightness of Phantom Lungs for Two Reductions in Lung Volume	
Photon Energy (MeV)	½ Voxel Reduction	1 Voxel Reduction
0.017	0.9576	0.9279
0.025	0.9785	0.9626
0.036	0.9845	0.9642
0.052	0.9968	0.9762
0.076	0.9974	0.9837
0.111	0.9817	0.9724
0.162	0.9856	0.9738
0.236	0.9927	0.9854
0.343	0.9766	0.9659
0.5	0.9953	0.9859

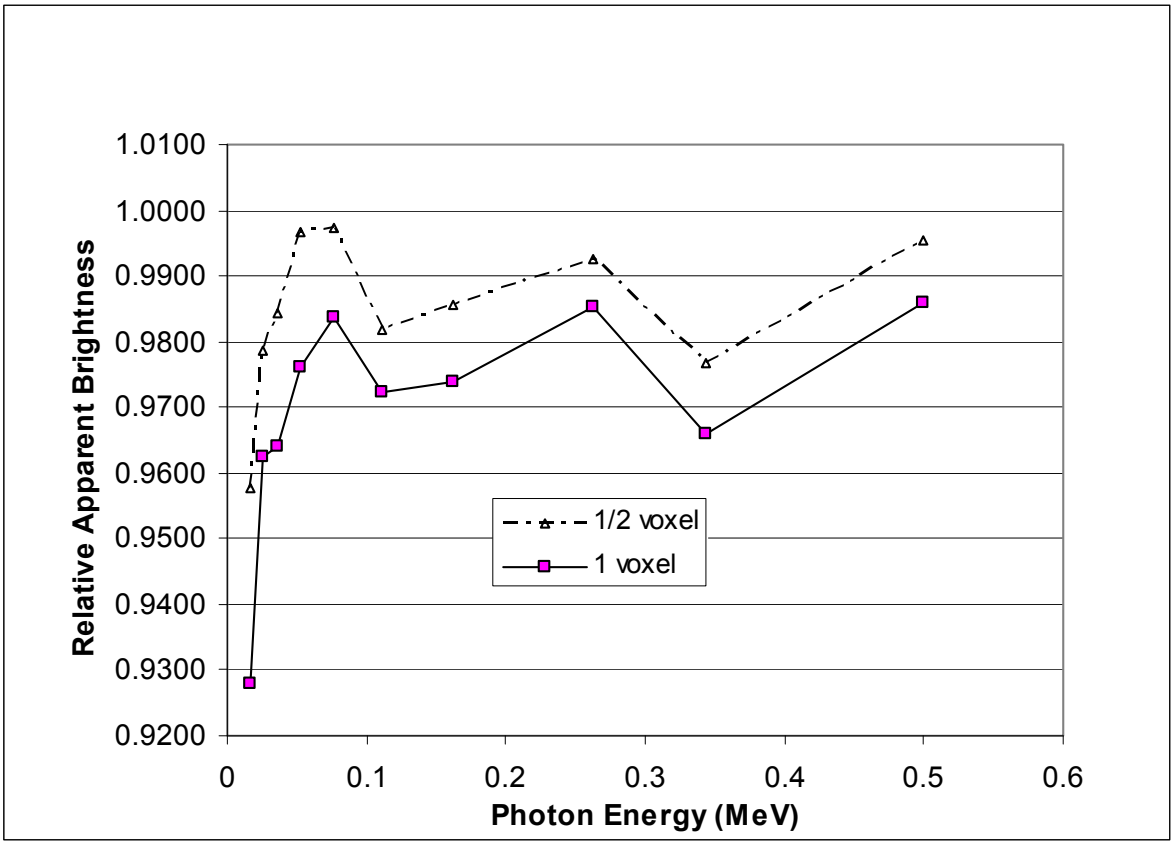

Figure 5.1. Influence of Phantom Lung Shrinkage on Relative Apparent Brightness

The calculations show a decrease in the relative apparent brightness for photons emitted from the smaller, but denser, phantom lungs. For both experiments, the reduction in apparent brightness was less than what would have been anticipated based on the density of the reduced lung. The effect was most pronounced in the case of the 1-voxel-thick air surface layer, where the density of the phantom lung material was 0.314 g cm^{-3}, but the relative apparent brightness of 0.017-MeV photons was more closely associated with a phantom lung density of 0.28 g cm^{-3}. In the case of a one-half voxel reduction, which more closely approximates the shrinkage that has been observed, the density of the shrunken lung was 0.2873 g cm^{-3} but the relative apparent brightness was more closely associated with a phantom lung density of 0.286 g cm^{-3}.

6.0 Skin Formation

The foams used at PNNL for phantom lung manufacture are self-skinning, which means that a thin skin is formed at the surface of the phantom lung that is slightly denser than the interior of the phantom lung. This numerical experiment was intended to estimate the extent to which the presence of a relatively high density skin would influence the brightness of a phantom lung. To make the determination, the density of the surface layer voxels was increased. To provide mass balance, the density of the lung material in the interior voxels was decreased. The activity in the surface layer of the phantom lung was also increased proportionately with the mass increase. The densities and activity fractions of the surface layer and interior regions of the phantom lungs are shown in Table 6.1.

Table 6.1. Experimental Set-up for Skin Study

	Density ($g\ cm^{-3}$)		Activity Fraction	
Code	Surface (Skin)	Interior	Surface (Skin)	Interior
N2[a]	0.26	0.26	0.17336	0.82664
S2[b]	0.20	0.272583	0.13335	0.86665
S3[b]	0.30	0.251611	0.20003	0.79997
S4[b]	0.40	0.230640	0.26671	0.73329
S5[b]	0.50	0.209668	0.33338	0.66662
S6[b]	0.60	0.188697	0.40006	0.59994
S7[b]	0.7	0.167726	0.46674	0.53326
S8[b]	0.8	0.146755	0.53341	0.46659
S9[b]	0.9	0.125783	0.60009	0.39991
26[c]	0.26	0.26	0	1

a. All voxels are 0.26 g cm^{-3}, but surface and interior voxels are differentiated (reference lung).

b. Test cases are two-part phantom lungs.

c. All voxels 0.26 cm^{-3}, but surface and interior voxels are not differentiated.

6.1 Methods

The skin layer was assumed to be one voxel thick and the surface voxels were identified as described in Section 3.3. The density of the skin ranged from 0.2 to 0.9 g cm^{-3}. The density of the interior of the phantom lung was adjusted to conserve mass. The activity in the surface layer was increased in proportion to the weight fraction of the phantom lung in the surface layer.

For this experiment, two versions of the reference lung were prepared. One reference phantom lung, designated 26 in Table 6.1, had no skin layer and the entire phantom lung had a density of 0.26 g cm^{-3}. The second reference phantom lung, designated N2 in Table 6.1, was a two-part lung that consisted of a surface layer and an inner region; both the surface layer and the inner region had a density of 0.26 g cm^{-3}. The purpose of using two types of phantom lungs was to determine if the segmentation of the phantom into two parts would have an influence on the calculated relative apparent brightness. The relative

apparent brightness of the two implementations of the phantom lung varied from 0.12% to about 6%, depending on the energy of the originating photon. The reason for the differences may be because the two regions were not sufficiently sampled by the Monte Carlo method or that the right and left lungs are not the same size and this might affect the calculations. There is no easy way to distinguish between right and left lungs in the Norman phantom because, in the phantom, the right and left lungs merge at certain locations, and so this hypothesis was not tested.

There was a difference between the two methods of calculating the brightness of the phantom lung that had no skin. The reason for the difference was not determined. To avoid any bias that might arise due to those differences, the segmented (two zone) phantom lungs were used as the basis for determining the relative apparent brightness.

6.2 Results

The results of the skin study are shown in Table 6.2. It can be seen that, in general, the increased skin density increases the brightness of the phantom lung possibly because the activity has been relocated from the interior of the phantom lung to the surface of the phantom lung and there is less material for the photons to traverse than for those photons that originate in the anterior region of the phantom lung. As can be seen in Table 6.2, the influence of a skin is relatively small unless there is a large difference in density when comparing the interior and surface of the phantom lung.

Table 6.2. Results from Skin Study

	Relative Apparent Brightness[a] Skin Density (g cm^{-3})							
Photon Energy (MeV)	0.2[b]	0.3	0.4	0.5	0.6	0.7	0.8	0.9
0.017	0.9827	0.9914	0.9897	1.0168	1.0407	1.0553	1.0522	1.0476
0.025	0.9925	0.9911	1.0048	1.0097	1.0134	1.0166	1.0118	1.0101
0.036	0.9926	0.9958	1.0059	1.0060	1.0039	1.0023	1.0004	0.9988
0.052	0.9980	1.0061	1.0125	1.0142	1.0170	1.0208	1.0226	1.0171
0.076	0.9945	1.0085	1.0076	1.0106	1.0099	1.0117	1.0091	1.0093
0.111	0.9969	1.0011	1.0101	1.0124	1.0070	1.0189	1.0215	1.0225
0.162	0.9951	0.9964	1.0034	1.0065	1.0091	1.0150	1.0139	1.0131
0.236	0.9945	1.0027	1.0110	1.0171	1.0171	1.0135	1.0150	1.0149
0.343	0.9987	0.9907	0.9975	1.0076	1.0128	1.0195	1.0218	1.0247
0.5	0.9978	1.0088	1.0221	1.0222	1.0281	1.0260	1.0303	1.0293

a. For these calculations, the basis phantom lungs used ALT2 as the lung tissue substitute and were partitioned into two regions: surface and interior.

b. Density of skin layer, g cm^{-3}.

Figure 6.1 is a three dimensional plot of the results and illustrates the observation that, in general, the relative apparent brightness increases as the density of the surface layer increases. It also shows that the response function is neither smooth nor entirely consistent.

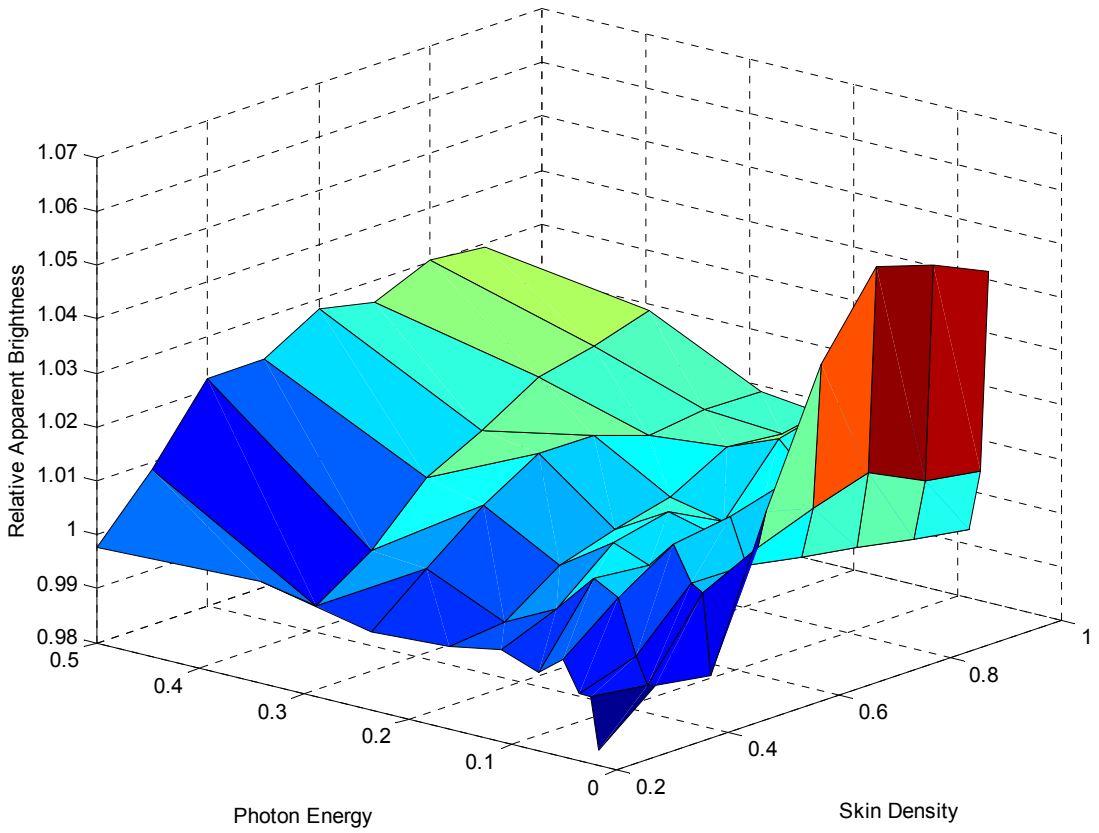

Figure 6.1. Influence of the Density of a Phantom Lung Surface Skin Layer on the Relative Apparent Brightness

7.0 Coating Study

Phantom lungs are coated with a polyurethane material to prevent spread of radioactive material and to provide some mechanical strength to the lungs to minimize crumbling and disintegration of the lungs. Because the coating contains no radioactive material, it will attenuate the photons emitted in the phantom lungs, and unlike skin formation it will not enhance the brightness of the lung by placing radioactivity close to the surface of the lung. This numerical experiment was intended to quantify the influence of the lung coating on the relative apparent brightness of a finished phantom lung.

7.1 Methods

The thickness of the protective coating of an actual phantom lung was measured with a micrometer and was found to range from 0.038 cm to 0.1524 cm. The coating is not uniformly thick for various reasons including the fact that the material is difficult to apply uniformly and the coating will sag due to gravity while drying. No attempt was made to perform a rigorous statistical analysis of the thickness of the coating on phantom lungs or to determine if the measured thickness of the coating of this one single phantom lung spanned the entire range of possible coating thicknesses. Based on the single phantom lung, it seems that, while some coating material does penetrate into the phantom lung, most of the coating is on the surface of the phantom lung.

With a voxel phantom it is not possible to simulate coating the phantom lung with an arbitrarily thick layer of a material. The thickness of any layer is determined by the size of the voxel, in this case approximately 2 mm. In order to test the influence of the coating layer on the surface of the voxel phantom lung, an approximation to the true situation was devised by assuming that the density of unexpanded lung tissue material is 1 g cm^{-3} and that the coating material soaks into the phantom lung material and fills the spaces (voids) in lung foam. The coating is also assumed to penetrate into only the first 2 mm of the phantom lung.

Surface layer voxels were identified as previously described. The surface layer is nominally 2 mm thick and the density of expanded lung tissue substitute is 0.26 g cm^{-3}. This implies that only 0.52 mm of the surface layer is required for the unexpanded lung tissue substitute. The remaining 1.48 mm of the surface layer is available for the coating material. The seal coating on the surface of the phantom lung was implemented by adjusting the elemental composition and density of the hybrid material on the surface of the phantom lung to account for the volume fractions of the lung tissue substitute and the lung sealant present in the surface voxels of the phantom lung. Table 7.1 lists the densities of the phantom lung surface layer and the equivalent coating thickness that were included in this study.

Table 7.1. Experimental Setup for the Voxel Phantom Calculations; Definition of Phantom Lung Surface Layer

Case Number	Transition Zone Density (g cm^{-3})	Assumed Coating Density (g cm^{-3})	Equivalent Thickness (cm)
C1	1.0	0.74	0.148
C2	0.63	0.37	0.074
C3	0.455	0.185	0.037

The validity of mixing the lung coating material and lung tissue substitute in the surface layer of the phantom lung and making an artificial transition zone of a hybrid material was investigated by performing two numerical experiments with a simplified spherical geometry. The first set of experiments, as summarized in Table 7.2, had seven different runs code named G0 through G6. The basis case, G0, simulated a phantom lung with no coating. The first set of experimental calculations used a distinct coating layer of varying thickness over the lung tissue substitute that formed the center of the sphere. For the final three runs (G4–G6), the lung sealant and the outer 2 mm of lung tissue substitute were merged to form a hybrid material whose elemental composition and density was determined by combining the volume adjusted combination of the lung tissue substitute and the phantom lung sealant. The calculations were run for 60 minutes to obtain good statistics. A f2 tally that reports the number of particles per cm^2 that crossed a surface of the spherical geometry was used for the calculations.

Table 7.2. Experimental Setup for Testing the Equivalence of Hybrid and Distinct Coating Layers

Geometry	Coating Thickness (cm)	Transition Zone Density (g cm^{-3})	Transition Zone Material (Volume fraction of material shown in parentheses)
G0	NA	0.26	synthetic lung(1)
G1	0.148	0.26	synthetic lung(1)
G2	0.074	0.26	synthetic lung(1)
G3	0.037	0.26	synthetic lung(1)
G4	equiv(0.148)	1.0	synthetic lung(0.26) + paint(0.74)
G5	equiv(0.074)	0.63	synthetic lung(0.41) + paint(0.59)
G6	equiv(0.037)	0.445	synthetic lung(0.58) + paint(0.42)

7.2 Results

The results of the validation study are shown in Table 7.3. Columns labeled "distinct layer" show the attenuation of the photons by a distinct layer of phantom lung sealant at three thicknesses. Columns labeled "Mixed Layer" show the attenuation by a 2-mm-thick hybrid layer that combines the lung tissue substitute and phantom lung sealant material. The data show that the two methods resulted in similar attenuation values for all energies. Even in the worst case, a combination of 0.037-cm lung sealant and 0.017-MeV photons, the difference between the two methods was only about 2%.

The attenuation of reference energy photons by phantom lung coating material is shown in Table 7.4. As stated previously, the actual thickness of the coating material on phantom lungs has not been determined. Visual observations that are based on slices of coated lungs indicate that thinner layers are more likely than thick layers. The data shown in Table 7.4 show that the coating can reduce the brightness of a phantom lung by up to 16% for low (0.017 MeV) energy photons. Even 0.076 cm of lung coating material will reduce the brightness of 0.017-MeV photons by 5%.

Table 7.3. Equivalence of Hybrid and Distinct Coating Layers

Photon Energy (MeV)	Relative Brightness of Spherical Sources					
	Distinct Layer			Mixed Layer		
	G1[a]	G2	G3	G4	G5	G6
0.017	0.8895	0.9299	0.9520	0.8896	0.9449	0.9722
0.025	0.9439	0.9635	0.9740	0.9400	0.9702	0.9848
0.036	0.9565	0.9729	0.9816	0.9552	0.9776	0.9885
0.052	0.9608	0.9766	0.9839	0.9604	0.9798	0.9899
0.076	0.9624	0.9782	0.9856	0.9617	0.9817	0.9908
0.111	0.9658	0.9801	0.9873	0.9643	0.9823	0.9906
0.162	0.9695	0.9815	0.9873	0.9680	0.9836	0.9921
0.236	0.9726	0.9837	0.9890	0.9715	0.9857	0.9929
0.343	0.9752	0.9845	0.9895	0.9747	0.9870	0.9933
0.5	0.9797	0.9879	0.9919	0.9787	0.9892	0.9947

a. Geometry descriptor as shown in Table 7.2.

Table 7.4. Results of the Calculations for the Voxel Phantom

Photon Energy (MeV)	Attenuation Relative to Unsealed Lung		
	C1[a]	C2	C3
0.017	0.8355	0.9090	0.9503
0.025	0.8956	0.9415	0.9684
0.036	0.9147	0.9531	0.9741
0.052	0.9170	0.9594	0.9826
0.076	0.9185	0.9579	0.9780
0.111	0.9302	0.9636	0.9826
0.162	0.9336	0.9655	0.9818
0.236	0.9363	0.9646	0.9808
0.343	0.9467	0.9733	0.9868
0.5	0.9514	0.9753	0.9886

a. Case number as shown in Table 7.1.

8.0 Linear Attenuation as a Predictor of Apparent Brightness

Not everyone has the desire or the ability to compute the relative apparent brightness of phantom lungs made from an arbitrary lung tissue substitute. The relatively straight lines obtained by the density study for the ALT2 material suggested that the linear attenuation coefficient would be a good surrogate for the apparent brightness. The purpose of this numerical experiment was to determine if all materials followed the same general line or if different materials had different lines.

8.1 Method

The relative apparent brightness and relative linear attenuation coefficient were calculated for every material-density-originating photon energy combination studied for this report, including the lung tissue substitutes described in Section 9.0. Relative linear attenuation coefficients were obtained by dividing the linear attenuation coefficient, without coherent scatter, of each lung tissue substitute by the linear attenuation coefficient, without coherent scatter, of ICRU-44 lung tissue at a density of 0.26 g cm^{-3}. Relative apparent brightness was calculated as previously described.

For all photon energies included in this study, linear regression parameters were calculated for every curve (relative apparent brightness as a function of relative linear attenuation coefficient) using the linear regression function of S-Plus 6.0. In the spirit of Occam's razor, the lowest order polynomial that provided a good fit to the data was reported. Keeping in mind Kant's recommendation that "The variety of beings should not rashly be diminished," the possibility of higher order polynomials was not ignored. (http://en.wikipedia.org/wiki/Occam's_Razor)

8.2 Results

The results of the regression calculations are listed in Table 8.1. The F and R^2 values of each fit are very large, indicating that the data are adequately fitted by the curve described.

Table 8.1. Regression Data for All Originating Photon Energies

Coefficients	Value	Std Error	t	R^2	Residual Std. Error	F
		0.017-MeV Photon; 3rd Order Polynomial				
Intercept	4.6234	0.1763	26.2186	0.9902	0.01812	3486
X	-7.0091	0.4643	-15.0958			
X^2	4.3697	0.4004	10.9134			
X^3	-0.9894	0.1127	-8.7759			
	0.025-MeV Photon; 1st Order Polynomial. Alderson Data Not Included					
Intercept	1.4396	0.0058	284.4118	0.9833	0.009184	5764
X	-0.4363	0.0057	-75.9240			

Table 8.1. (contd)

Coefficients	Value	Std Error	t	R^2	Residual Std. Error	F
0.025-MeV Photon; 2nd Order Polynomial. Alderson Data not Included.						
Intercept	1.6096	0.0102	157.5445	0.9959	0.004559	11850
X	-0.7679	0.0193	-39.7156			
X^2	0.1575	0.0091	17.3404			
0.036-MeV Photon; 1st Order Polynomial						
Intercept	1.3013	0.0025	515.3051	0.9929	0.004191	14610
X	-0.3008	0.0025	-120.8780			
0.052-MeV Photon; 1st Order Polynomial						
Intercept	1.2542	0.0024	526.3363	0.9909	0.004114	11430
X	-0.2515	0.0024	-106.9152			
0.076-MeV Photon; 1st Order Polynomial. s06 Data not included.						
Intercept	1.2240	0.0019	639.7755	0.9926	0.003341	13760
X	-0.2225	0.0019	-117.3159			
0.076-MeV Photon 1st Order Polynomial.						
Intercept	1.2246	0.0025	481.6155	0.9867	0.0045	7810
X	-0.2226	0.0025	-88.3747			
0.111-MeV Photon; 1st Order Polynomial						
Intercept	1.2064	0.0013	915.5949	0.9957	0.002352	24140
X	-0.2033	0.0013	-155.5380			
0.162-MeV Photon; 1st Order Polynomial.						
Intercept	1.1791	0.0012	944.6250	0.9950	0.002237	20860
X	-0.1797	0.0012	-144.4337			
0.236-MeV Photon; 1st Order Polynomial.						
Intercept	1.1607	0.0009	1233.5708	0.9965	0.001691	29520
X	-0.1603	0.0009	-171.8176			
0.343-MeV Photon; 1st Order Polynomial.						
Intercept	1.1473	0.0009	1299.3178	0.9964	0.001585	28800
X	-0.1487	0.0009	-169.7136			
0.500-MeV Photon; 1st Order Polynomial						
Intercept	1.1303	0.0008	1401.7180	0.9960	0.001451	25960
X	-1.1294	0.0008	-161.1274			

Plots of the data are shown in Figure 8.1 to Figure 8.11. The plots show that there are some outlying data points at certain photon energies but the number of outliers is few and there appears to be no systematic errors. The plots also show that, while there is some difference between materials, as evidenced by the variation in the data, there is good agreement among all the materials studied in that the data for all materials, with two exceptions, are described by the same line. For 0.025-MeV photons, the relative apparent brightness and relative linear attenuation coefficient relationship of the Alderson lung tissue substitute is described by a line different than for the other lung tissue substitutes. For 0.076-MeV photons, the outlying material is a designed lung tissue substitute that contains BiO_2. In the case of 0.343-MeV photons, both apparent outliers have a density of 0.32 g cm^{-3} but are different materials.

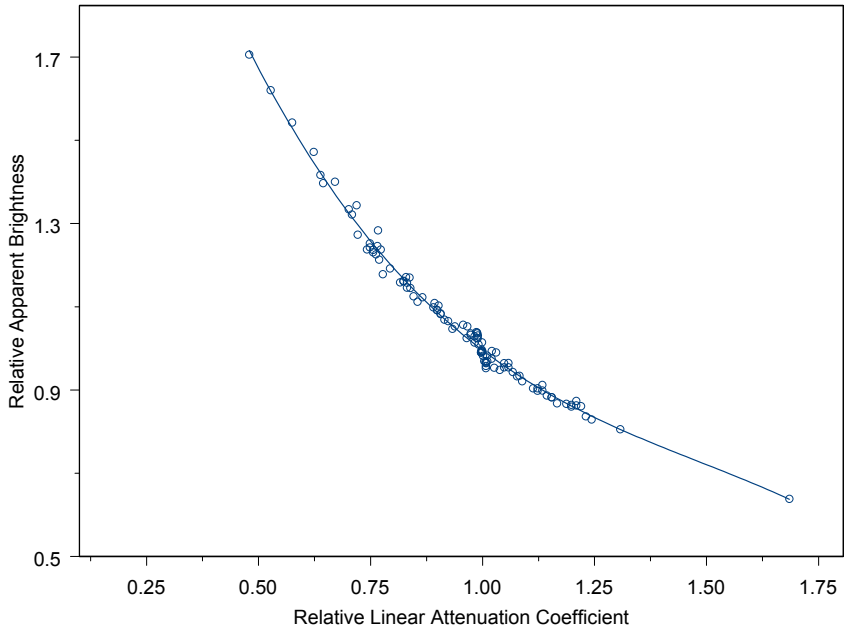

Figure 8.1. Relative Apparent Brightness of Phantom Lungs as a Function of the Relative Linear Attenuation Coefficient (0.017 MeV). The energy of the originating photons was 0.017 MeV. The equation that describes the data is a third-order polynomial.

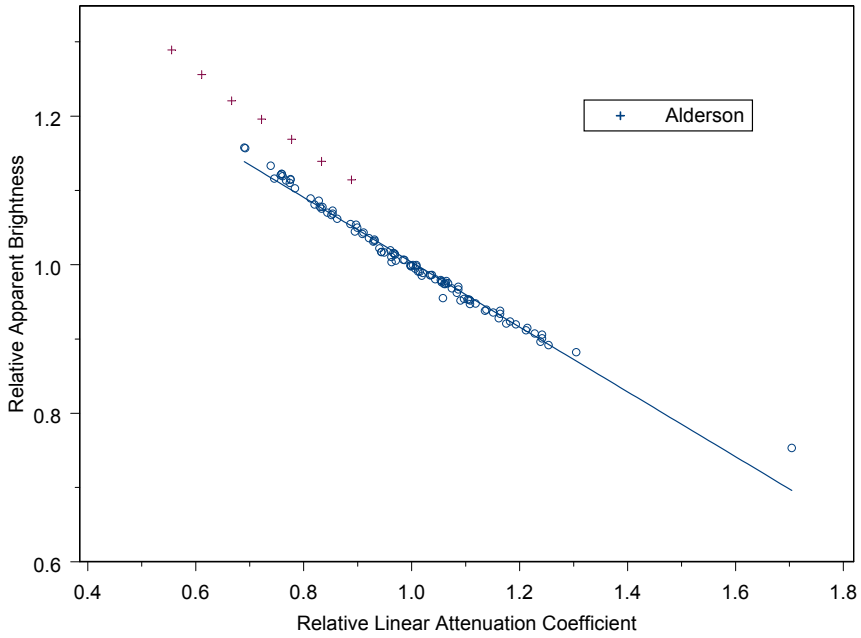

Figure 8.2. Relative Apparent Brightness of Phantom Lungs as a Function of the Relative Linear Attenuation Coefficient (0.025 MeV). The Energy of the originating photon was 0.025 MeV. The equation that describes the data is a first-order polynomial. The Alderson data were not included in the calculation of the fitting equation.

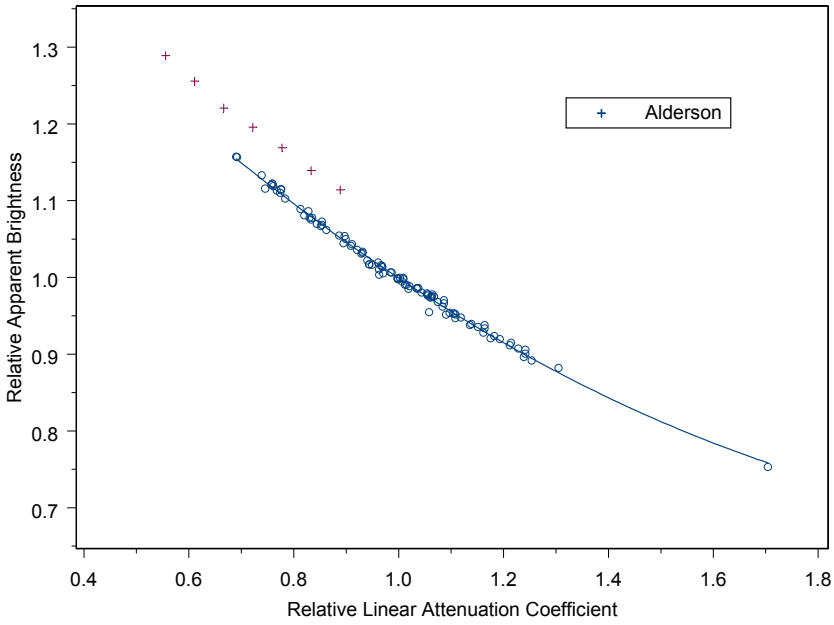

Figure 8.3. Relative Apparent Brightness of Phantom Lungs as a function of the Relative Linear Attenuation Coefficient (0.025 MeV). The energy of the originating photon was 0.025 MeV. The equation that describes the data is a second-order polynomial. The Alderson data were not included in the calculation of the fitting equation.

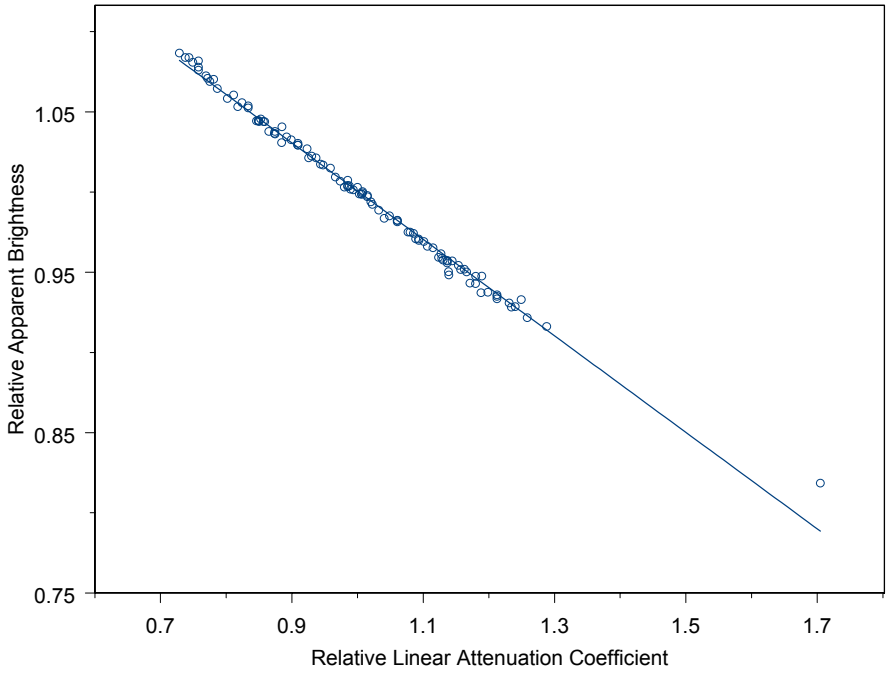

Figure 8.4. Relative Apparent Brightness of Phantom Lungs as a Function of the Relative Linear Attenuation Coefficient (0.036 MeV). The energy of the originating photon was 0.036 MeV. The equation that describes the data is a first-order polynomial.

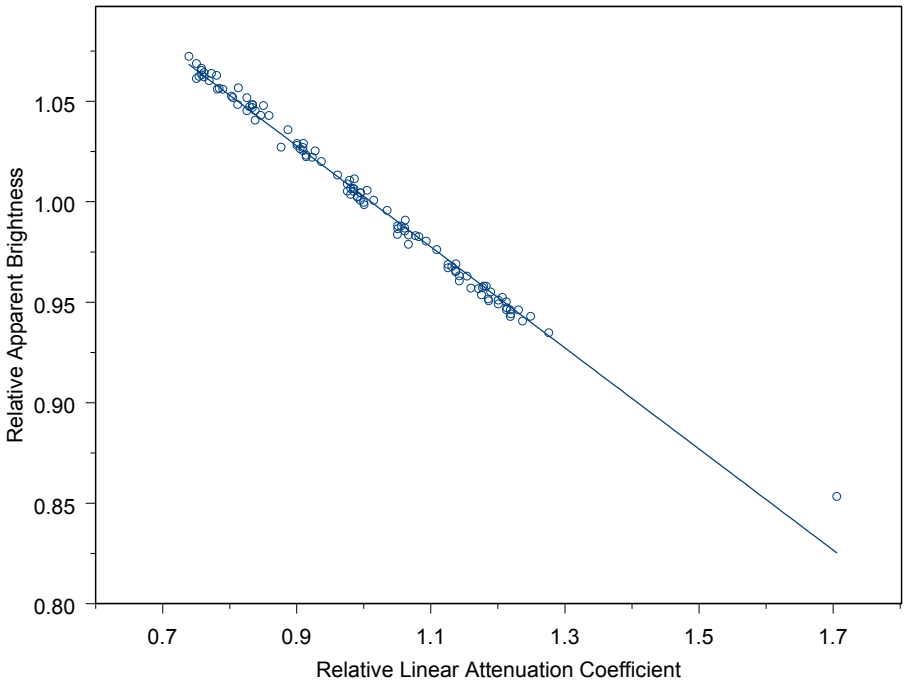

Figure 8.5. Relative Apparent Brightness of Phantom Lungs as a Function of the Relative Linear Attenuation Coefficient (0.052 MeV). The energy of the originating photon was 0.052 MeV. The equation that describes the data is a first-order polynomial.

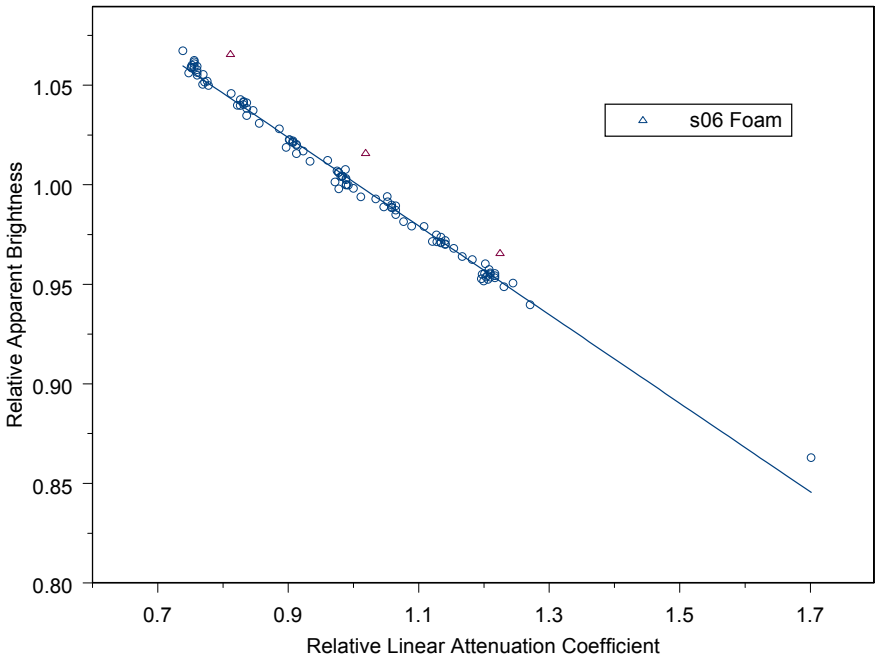

Figure 8.6. Relative Apparent Brightness of Phantom Lungs as a Function of the Relative Linear Attenuation Coefficient (0.076 MeV). The energy of the originating photon was 0.076 MeV. The equation that describes the data is a first-order polynomial. The s06 lung material data were not included in the calculation of the fitting equation.

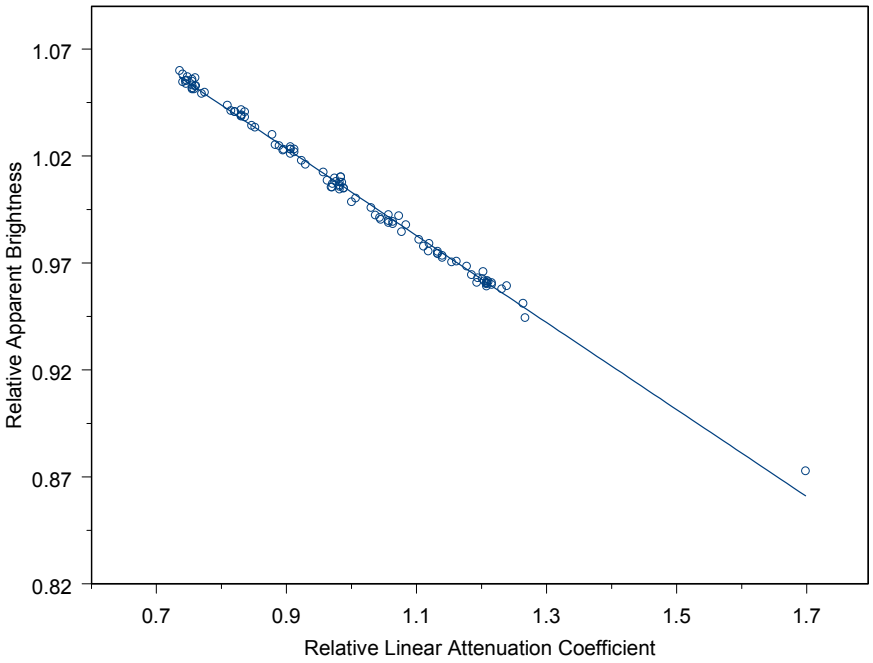

Figure 8.7. Relative Apparent Brightness of Phantom Lungs as a Function of the Relative Linear Attenuation Coefficient (0.111 MeV). The energy of the originating photon was 0.111 MeV. The equation that describes the data is a first-order polynomial.

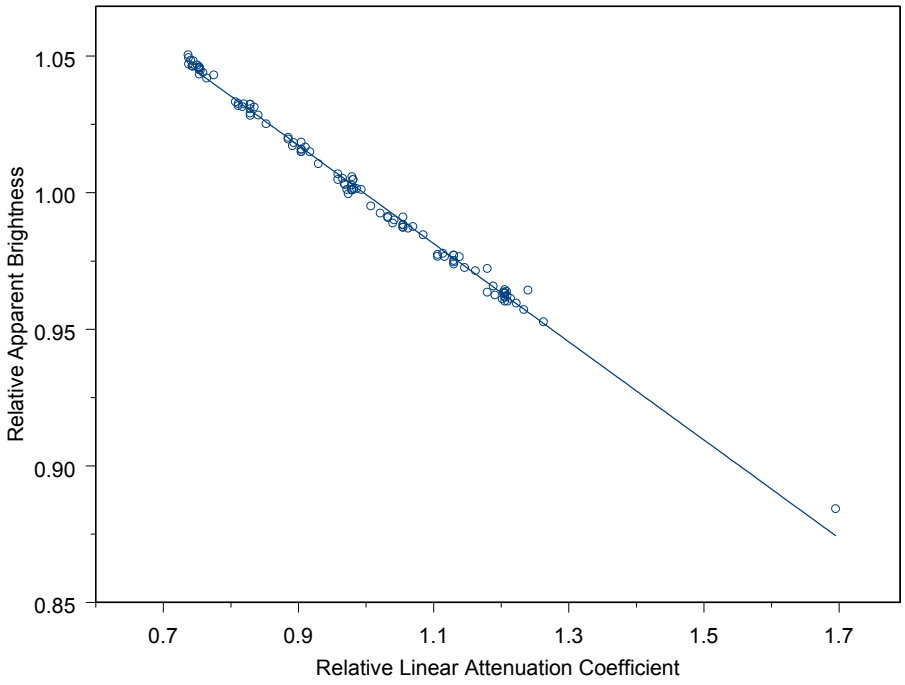

Figure 8.8. Relative Apparent Brightness of Phantom Lungs as a Function of the Relative Linear Attenuation Coefficient (0.162 MeV). The energy of the originating photon was 0.162 MeV. The equation that describes the data is a first-order polynomial.

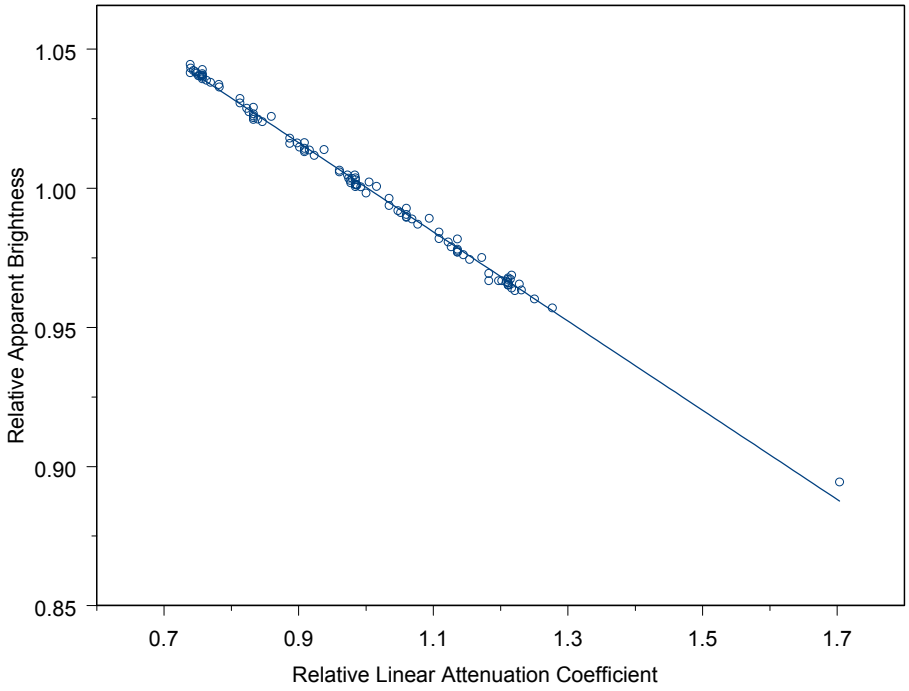

Figure 8.9. Relative Apparent Brightness of Phantom Lungs as a Function of the Relative Linear Attenuation Coefficient (0.236 MeV). The energy of the originating photon was 0.236 MeV. The equation that describes the data is a first-order polynomial.

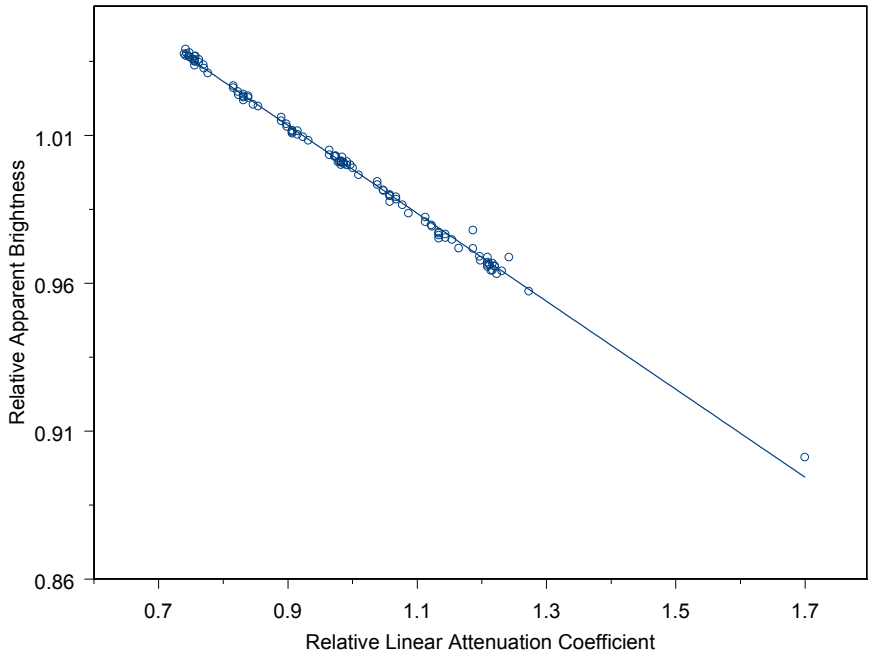

Figure 8.10. Relative Apparent Brightness of Phantom Lungs as a Function of the Relative Linear Attenuation Coefficient (0.343 MeV). The energy of the originating photon was .0343 MeV. The equation that describes the data is a first-order polynomial.

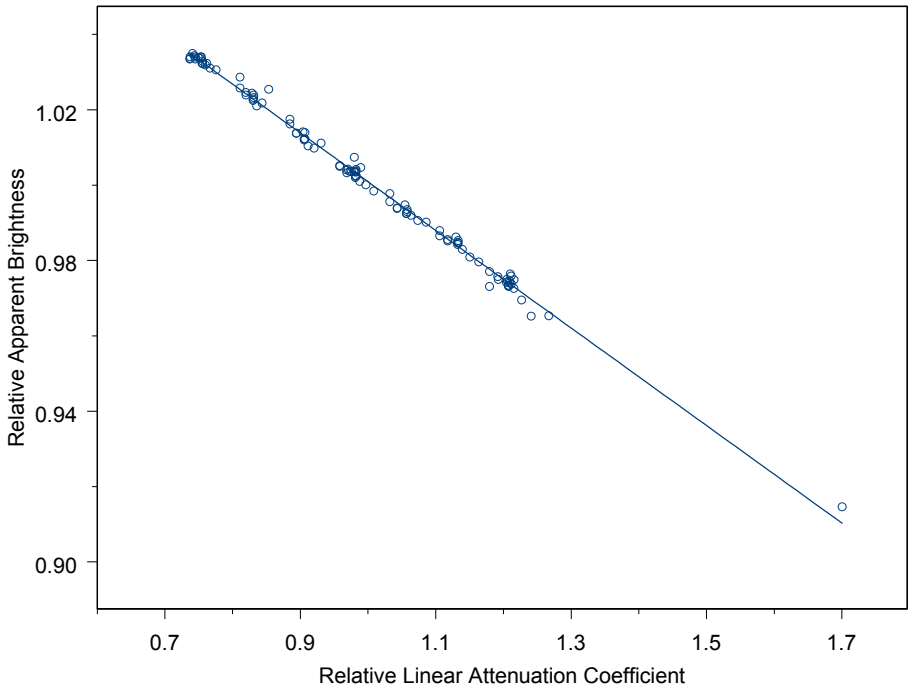

Figure 8.11. Relative Apparent Brightness of Phantom Lungs as a Function of the Relative Linear Attenuation Coefficient (0.500 MeV). The energy of the originating photon was 0.500 MeV. The equation that describes the data is a first-order polynomial.

9.0 Linear Attenuation Coefficients as an Aid to Design of Lung Tissue Substitutes

Some foaming plastics used to manufacture phantom lungs might not achieve a density of 0.26 g cm^{-3}. In the previous section it was shown that the linear attenuation coefficient of the lung tissue substitute would provide an indication of how close the performance of a given lung tissue substitute would match the performance of the reference lung tissue. To test the usefulness of the linear attenuation coefficient for design of lung tissue substitutes, the following experiment was performed to determine the ability of the linear attenuation coefficient to adjust the amount of adjuvant incorporated into a phantom lung.

9.1 Methods

To further test the hypothesis that the linear attenuation coefficient was a good predictor of the performance of a phantom lung, an experiment was performed with polyurethane augmented by seven adjuvants, listed in Table 9.1. For this experiment, the ratio of the two components, (i.e., polyurethane and adjuvant) was determined by choosing the weight fraction of the adjuvant in the lung tissue substitute that minimized the sum of the squares of the difference between the linear attenuation coefficients of the designed lung tissue substitute and the reference lung tissue for all 10 photon energies. Three densities of lung tissue substitute were chosen: 0.2, 0.26, and 0.32 g cm^{-3}. Table 9.2 lists the weight fraction of the adjuvants in the experimental lung tissue substitutes. The linear attenuation coefficients both with and without coherent scatter were used to calculate the amount of adjuvant that would be added.

Table 9.1. Adjuvants Used for the Lung Tissue Substitute Design Experiment

Adjuvant number	Adjuvant
00	Al_2O_3
01	$Al(OH)_3$
02	SiO_2
03	$CaCO_3$
04	tris(2-chloroethyl) phosphate
05	Type 04 concrete
06	Bi_2O_3

9.2 Results

The results of these calculations are shown in Table 9.3. The data show that, at a density of 0.26 g cm^{-3}, all adjuvants except Bi_2O_3 can be used to design a lung tissue substitute whose relative apparent brightness is within 1% of the reference lung tissue. When the lung tissue substitute has a density of 0.2 g cm^{-3} or 0.32 g cm^{-3}, a difference of 23% compared to the density of the reference lung tissue, the apparent brightness of the designed lung tissue substitute is still within 5% of the reference lung tissue. Observation of the data in Table 9.2 indicates an inverse relationship between density of lung tissue substitute and its relative apparent brightness in that a designed lung tissue substitute whose density is

greater than 0.26 g cm^{-3} will tend to be brighter than expected and a lung tissue substitute whose density is less than 0.26 g cm^{-3} will tend to be less bright than expected. Interestingly, the relationship observed for nearly all photon energies is reversed for 0.017-MeV photons. The data indicate that it is easier to match the reference lung tissue when the density of the lung tissue substitute is about the same density as the reference. The data also show that the inclusion of coherent scatter in the linear attenuation coefficient does not greatly influence the predictive value of the linear attenuation coefficient.

Table 9.2. Weight Fraction of Adjuvant Added to Lung Tissue Substitute to Prepare a Lung Tissue Substitute

This table shows the weight fraction of adjuvant (see previous table) that was added to the Foamex material in order to obtain the optimal (by least squares) mix of adjuvant and Foamex for three different lung tissue substitute densities.

	Weight Fraction of Adjuvant		
Density Foam Number[a]	0.20 g cm^{-3}	0.26 g cm^{-3}	0.32 g cm^{-3}
	Based on Linear Attenuation Coefficient without Coherent Scatter		
S00	0.301	0.168	0.085
S01	0.426	0.238	0.121
S02	0.253	0.141	0.071
S03	0.098	0.055	0.028
S04	0.156	0.087	0.044
S05	0.163	0.091	0.046
S06	0.007	0.004	0.002
	Based on Linear Attenuation Coefficient with Coherent Scatter		
C00	0.311	0.171	0.083
C01	0.440	0.241	0.117
C02	0.263	0.144	0.070
C03	0.104	0.057	0.027
C04	0.164	0.090	0.043
C05	0.171	0.094	0.045
C06	0.007	0.004	0.002

a. Foam number: the letter indicates calculations based on linear attenuation coefficient with (c) or without (s) coherent scatter. The two digits refer to the adjuvant listed in Table 9.1.

Table 9.3. Fractional Difference in Apparent Brightness for Phantom Lungs Made of Enhanced Lung Tissue Substitute Compared to Apparent Brightness of ICRU-44 Lung Tissue

	Phantom Lung Density (g cm^{-3})					
	0.2	0.26	0.32	0.2	0.26	0.32
Photon Energy (MeV)		C00[a]			C01	
0.017	0.055	0.014	-0.040	0.053	0.015	-0.024
0.025	-0.011	0.005	0.019	-0.008	0.005	0.020
0.036	-0.042	0.002	0.040	-0.039	0.005	0.043
0.052	-0.058	-0.004	0.046	-0.051	-0.002	0.046
0.076	-0.058	-0.009	0.042	-0.062	-0.003	0.049
0.111	-0.058	-0.008	0.039	-0.055	-0.008	0.039
0.162	-0.051	-0.003	0.035	-0.047	0.000	0.042
0.236	-0.044	-0.005	0.031	-0.046	-0.005	0.029
0.343	-0.037	-0.003	0.035	-0.037	-0.001	0.034
0.5	-0.035	-0.006	0.023	-0.038	-0.007	0.023
		C02			C03	
0.017	0.068	0.009	-0.046	0.059	0.023	-0.052
0.025	-0.006	0.001	0.018	0.012	0.017	0.025
0.036	-0.033	0.006	0.041	-0.027	0.004	0.043
0.052	-0.056	-0.005	0.041	-0.049	0.004	0.046
0.076	-0.065	-0.007	0.048	-0.053	-0.002	0.042
0.111	-0.058	-0.008	0.037	-0.053	-0.009	0.041
0.162	-0.044	0.001	0.038	-0.044	-0.003	0.041
0.236	-0.046	-0.005	0.031	-0.045	-0.005	0.033
0.343	-0.038	-0.001	0.036	-0.036	-0.001	0.035
0.5	-0.038	-0.007	0.023	-0.037	-0.006	0.025
		C04			C05	
0.017	0.065	0.030	-0.039	0.057	0.030	-0.031
0.025	0.007	0.015	0.026	-0.003	0.014	0.025
0.036	-0.036	0.002	0.046	-0.032	0.001	0.049
0.052	-0.051	-0.004	0.044	-0.053	-0.003	0.044
0.076	-0.049	0.000	0.045	-0.053	-0.002	0.043
0.111	-0.051	-0.010	0.036	-0.055	-0.005	0.040
0.162	-0.048	-0.002	0.038	-0.046	-0.005	0.039
0.236	-0.041	-0.001	0.036	-0.042	-0.003	0.036
0.343	-0.036	-0.001	0.034	-0.037	-0.001	0.033
0.5	-0.035	-0.002	0.027	-0.034	-0.004	0.026
		C06				
0.017	0.046	0.023	-0.026			
0.025	0.045	0.048	0.051			
0.036	-0.002	0.028	0.060			
0.052	-0.028	0.015	0.055			
0.076	-0.067	-0.014	0.037			
0.111	-0.030	0.009	0.050			
0.162	-0.033	0.006	0.042			
0.236	-0.036	0.000	0.037			
0.343	-0.033	0.000	0.035			
0.5	-0.032	-0.002	0.028			

a. Foam number of Table 9.2.

Table 9.3. (contd)

	Phantom Lung Density (g cm^{-3})					
	0.2	0.26	0.32	0.2	0.26	0.32
Photon Energy (MeV)		S00[a]			S01	
0.017	0.042	0.007	-0.038	0.036	0.007	-0.031
0.025	-0.017	0.001	0.021	-0.017	0.003	0.024
0.036	-0.044	-0.004	0.039	-0.044	-0.002	0.041
0.052	-0.056	-0.011	0.046	-0.057	-0.004	0.043
0.076	-0.060	-0.007	0.045	-0.062	0.002	0.048
0.111	-0.058	-0.007	0.037	-0.055	-0.010	0.034
0.162	-0.051	-0.003	0.039	-0.049	-0.001	0.036
0.236	-0.043	-0.004	0.034	-0.042	-0.002	0.033
0.343	-0.038	-0.003	0.031	-0.038	-0.001	0.033
0.5	-0.033	-0.004	0.026	-0.035	-0.004	0.026
		S02			S03	
0.017	0.048	0.010	-0.039	0.030	0.003	-0.036
0.025	-0.016	0.001	0.022	-0.005	0.011	0.025
0.036	-0.044	-0.001	0.042	-0.031	0.002	0.043
0.052	-0.056	-0.007	0.042	-0.048	0.001	0.045
0.076	-0.058	-0.004	0.045	-0.052	0.000	0.043
0.111	-0.057	-0.008	0.038	-0.053	-0.008	0.039
0.162	-0.046	0.000	0.037	-0.045	-0.002	0.040
0.236	-0.042	-0.004	0.035	-0.041	-0.001	0.036
0.343	-0.037	-0.001	0.034	-0.037	0.000	0.033
0.5	-0.034	-0.004	0.027	-0.034	-0.002	0.026
		S04			S05	
0.017	0.034	0.010	-0.025	0.032	0.018	-0.024
0.025	-0.003	0.009	0.026	-0.010	0.010	0.022
0.036	-0.038	0.001	0.050	-0.037	0.001	0.052
0.052	-0.052	-0.004	0.049	-0.053	-0.001	0.048
0.076	-0.051	0.000	0.048	-0.055	-0.008	0.046
0.111	-0.051	-0.010	0.038	-0.051	-0.008	0.039
0.162	-0.046	-0.005	0.038	-0.047	-0.001	0.036
0.236	-0.040	-0.001	0.031	-0.040	-0.005	0.033
0.343	-0.037	-0.001	0.035	-0.036	-0.003	0.036
0.5	-0.034	-0.004	0.024	-0.034	-0.007	0.024
		S06				
0.017	0.047	0.025	-0.015			
0.025	0.045	0.048	0.053			
0.036	-0.003	0.029	0.063			
0.052	-0.027	0.016	0.056			
0.076	-0.065	-0.016	0.035			
0.111	-0.030	0.008	0.049			
0.162	-0.033	0.007	0.043			
0.236	-0.036	-0.002	0.034			
0.343	-0.033	0.000	0.037			
0.5	-0.032	-0.005	0.025			

b. Foam number of Table 9.2.

10.0 Discussion

10.1 Radiological Properties

Figures 3.1 to 3.6 show some variation in brightness as a function of the radiological properties studied but no trends can be seen that would allow the radiological properties to be used to predict how well a lung tissue substitute would perform, using relative apparent brightness as the performance metric. The plots of relative apparent brightness show that three lung tissue substitutes, Alderson Lung tissue substitute, A-150 and LLLL1, differ from the other lung tissue substitutes in that they show a significant trend at low energies. Plots of the relative apparent brightness as a function of photon energy for those three materials, not shown here, are flat at high photon energies and then show elevations at low photon energies.

The conclusion is that I, Z_{eff}, and n_0 cannot be used to predict the ability of a lung tissue substitute to exhibit the same performance as human lung tissue.

10.2 Density Study

The data shown in Figure 4.2 indicate that control of phantom lung density is crucial for phantom lungs that will be used for calibration and testing of chest-counting systems. PNNL is currently refining its manufacturing techniques in an attempt to control the variability of lung tissue densities to within ± 0.005 g cm^{-3} of the desired density.

The density range of phantom lungs in use at various chest-counting systems cannot be determined. Other authors have stated that their lung densities may range from 0.25 to 0.3 g cm^{-3} (Fry and Summerling 1982; Griffith et al. 1979). Spitz et al. (1994) do not state the densities of their lung tissue substitute but do indicate a 7% difference in linear attenuation coefficients for two lungs. If the slopes of the relative brightness line are identical for all lung tissue substitutes, this would imply a 9 to 16% difference in the brightness of the lungs, depending on the manufacturer.

Figure 4.1 shows why it is useful to use an indicator radionuclide to quantify intakes of radionuclides that emit low energy photons; the relative apparent brightness is less sensitive to phantom lung density variations at higher photon energies than at lower photon energies. An example of an indicator radionuclide is to use ^{241}Am as an indicator for intakes of ^{239}Pu when the relative activities of ^{241}Am and ^{239}Pu are known. But a tracer may not always be present, especially in testing phantom lungs.

10.3 Lung Shrinkage Study

Phantom lungs may shrink upon removal from the molds. The exact cause of the shrinkage was not investigated because the lung tissue substitute presently used at PNNL does not exhibit noticeable shrinkage. The results of lung shrinkage are that the density of the phantom lung increases and the brightness of the phantom lung decreases.

Of the photon energies studied, the maximal brightness reduction occurs for 0.017-MeV photons where the relative apparent brightness of the phantom lungs can be reduced by 4 to 7%, depending on the amount of shrinkage.

10.4 Skin Formation

The data show small variations in the relative apparent brightness for different skin thicknesses. The differences are not large and what differences that do occur are on the same order of the differences between the two methods of calculating the base brightness and are pronounced only when the thickness of the skin is approximately 2 mm. This thickness is greater than what has been observed.

Figure 6.1 is a surface plot of the data in Table 6.2 and shows little structure except that the 0.017-MeV peak shows a marked increase in the relative apparent brightness as the thickness of the skin layer increases. All photon energies show a small increase in the relative apparent brightness as the thickness of the skin increases. It should be noted that the trend is not monotonic. The density of the skin of a real phantom lung has not been quantified but, based on observation, it seems that the skin density is not greater than about 0.5 (an approximate doubling of the phantom lung density) in which case, the difference between the "no skin" phantom lung and the "with skin" phantom lung is about 2%. Even in the worst case, when the skin density ranges from 0.7 to 0.8 g cm^{-3}, the apparent brightness of phantom lungs with a skin is only about 5% greater than the apparent brightness of phantom lungs that lack a skin.

10.5 Linear Attenuation Prediction

The plots and statistics of the linear regressions indicate that the relative linear attenuation coefficient is an adequate metric for determining whether a particular lung tissue substitute can be used for phantom lungs. The figures show that the performance of a large number of different formulations of lung tissue substitutes will be similar to the performance of ICRU-44 average lung tissue. The data also imply that a large number of adjuvants can be added to the polyurethane base material to obtain an acceptable lung tissue substitute.

The slopes of the curves increase as the energy of the originating photons decrease. At higher photon energies, it appears that the relationship between the relative linear attenuation coefficient and the relative apparent brightness is linear but curvature is introduced into the relationship as the originating photon energy decreases. The possibility that the curvature observed for 0.017- and 0.025-MeV photons may be because the large dynamic range of the relative linear attenuation coefficient was not investigated. At higher photon energies, the dynamic range is narrower and the underlying curvature may have been masked. Indeed, the data point for LN300 at a density of 0.45 g cm^{-3} is seen as an apparent outlier but whose position could be explained by increasing the order of polynomial used to describe the relationship. At the same time, however, it is observed that, for 0.017-MeV photons, curvature is apparent even when the data are limited to include only those observations where the relative linear attenuation coefficient ranges from 0.7 to 1.25. In addition, the apparent outlying LN300 at a density of 0.45 g-cm^{-3} data appears to come closer to the straight line that describes the remaining data as the energy of the originating photon increases.

The linear attenuation coefficient of any particular material is a linear function of the material's density and these data reemphasize how important it is for the phantom lung manufacturer to control and especially to know the density and elemental composition of the phantom lungs and that this importance increases as the energy of the originating photon decreases. Other counting geometries will likely change the slope of the relationships described here, but the basic form of the relationships will be similar to those shown here.

The reason that the curves of the Alderson lung tissue substitute do not match the curves of other lung tissue substitutes at 0.017 and 0.027 MeV is not known. It may be related to the amount of Sb added. The original Griffith lung tissue substitute contains a small amount of Sn and does not exhibit anomalies, and Sn and Sb are adjoining elements on the periodic table. Because the anomalies are associated with moderately high Z number elements, it can be concluded that adjuvant materials should be limited to lower Z materials such as Ca, Mg, and Si.

All plots show a data point at a relative linear attenuation coefficient of about 1.7. In all cases this data point is due to LN300 at a density of 0.45 g cm-3. The data points do not fall on the curve when a straight line is fitted to the data. Although higher order polynomials were not fitted to the data, the location of the data point argues for the possibility that all curves are described by a second or third order polynomial. Higher order polynomials were not investigated because, in the region of interest, say, +\- 10% density range, a straight line adequately fits the data.

The data indicate that the relative linear attenuation coefficient of phantom lungs is a good, but not perfect, indicator of how well the phantom lungs will perform, as quantified by the relative apparent brightness. It appears that if the relative linear attenuation ranges from 0.95 to 1.05, then the relative apparent brightness of the phantom lungs will also range from 0.95 to 1.05. The linear attenuation coefficient of phantom lungs is readily obtained because the elemental composition of the lung tissue substitute is known to the phantom manufacturer and thus the mass attenuation coefficient is also known. The density of phantom lungs is readily obtained from the mass of the lung and its volume.

10.6 Adjuvant Additions

The following observations are made:

1. The chosen adjuvant is not critical except that it appears that high Z materials, such as BiO_2, make it more difficult to get a good match between the reference lung material and the lung tissue substitute.
2. The best match in relative apparent brightness between the reference lung tissue and the lung tissue substitutes occurs when the density of the two materials are the same.
3. The difficulty in obtaining a good match for all energies does not prevent the lung tissue substitute manufacturer from obtaining an excellent match for a limited range of photon energies. It seems possible to use the photon energies of interest as a guide to the optimal amount of adjuvant added to the lung tissue substitute. Referring back to Table 1.1, we see that each testing category has a different photon energy range. Thus it would be possible to adjust the lung tissue substitute to accommodate variations in the linear attenuation coefficient as a function of photon energy.

The results of this study show that a wide variety of adjuvants can be used to provide a good match between a lung tissue substitute and ICRU-44 normal adult lung tissue. Not only that, but it appears that no single adjuvant has a significant advantage over any other adjuvant, thus the phantom lung manufacturer can choose an adjuvant based on properties such as solubility, ease of providing a uniform distribution in the lung tissue substitute, chemical toxicity, or other criteria rather than based on a need to utilize a specific chemical entity to agree with historic practices.

Furthermore, the data show that a good match can be obtained even when the density of the lung tissue substitute is significantly different than the density of human lung tissue. This study did not consider how the adjuvant would influence the density of the lung tissue substitute as the quantity added was varied. Neither does this study consider whether lung tissue substitutes that contain any of the adjuvants in any concentration would be sufficiently robust to withstand continual use. These latter items would be for the lung tissue substitute manufacturer to determine.

The data show that using the linear attenuation coefficient of the components of lung tissue substitutes to design lung tissue substitutes can result in a lung tissue substitute that has a relative apparent brightness that is closer to unity than would be expected based on the differences in density. Using a density of 0.26 g cm^{-3} as the basis, the densities vary by 23%. If the amount of adjuvant added to the foam material remained constant, then the variation in linear attenuation would also vary by 23%. But the design scheme described here has reduced the variation to 6.5% or less. The relative apparent brightness for specific photon energies could be made closer to unity by performing the design calculations at the photon energies of interest. The data also show that the design criteria are most effective when the density of the lung tissue substitute is 0.26 g cm^{-3}, the same density of the reference material. This method can also be used as a quick way to develop new formulations of lung tissue substitutes when and if the plastic manufactures change the elemental composition of their formulations.

10.7 Protective Coating

It is difficult to estimate the influence of a protective coating on the relative apparent brightness of any particular phantom lung because the thickness of the coating can vary over the surface of the lung. After these calculations were performed, the author obtained data available from laser scans of the original plaster lung casts that were used for the Livermore Phantom. The data indicate that the surface area of the right lung is 1154.5 cm^2 and of the left lung 958.8 cm^2. The author also found pre- and post-painting masses of two sets of phantom lungs. The data indicate that the actual coating thickness for those lungs ranged from 0.0247 g cm^2 to 0.0271 g cm^2. These data indicate that the attenuation of 0.017-MeV photons may be as little as 4% for these lung sets. The quotient of the mass of coating material applied to the phantom lung divided by the surface area of the phantom lung provides a good estimate of the thickness of the coating and the resulting reduction in relative apparent brightness of the coated phantom lungs.

11.0 Conclusions

Various manufacturing processes were found to alter the relative apparent brightness of phantom lungs. The largest variations in relative apparent brightness are introduced by variations in density, a factor that can be readily quantified. All phantom lung manufacturing laboratories should attempt to estimate the relative apparent brightness of their phantom lungs. At the very least, the manufacturing laboratory should report the density and elemental composition of their phantom lungs.

The influence of some manufacturing processes on the performance of the phantom lungs may be unknowable because the only way to determine the influence is by direct measurement. The variations in relative apparent brightness can be fairly small and the inherent variability of chest-counting systems may be too large to quantify the interprocess differences in phantom lung performance.

For example, consider the influence of skin formation. A foaming material is either self-skinning or it is not. The only way to determine the influence of the skin formation process would be to make phantom lungs of self-skinning material and a non self-skinning material and measure the differences. But, the inherent variability caused by confounders such as variations in density, elemental composition, activity present in the lung would likely make it impossible to isolate the influence due to the skin.

This work also showed that a large number of lung tissue substitutes can be used to manufacture phantom lungs and still achieve a performance identical to a reference lung material. The single most important metric appears to be the linear attenuation coefficient of the phantom lung tissue substitute. If the linear attenuation coefficients of two lung tissue substitutes are identical, then it appears that the performance of phantom lungs made from those two materials, as quantified by their relative apparent brightness, will also be identical.

Figure 4.3 is a plot of the counting efficiency of the chest-counting system as a function of photon energy. It can be seen that the maximum counting efficiency is for photons whose energy is about 0.111 MeV. We say about because we have shown the most efficient photon energy of those included in the study, but not all possible photon energies in the region.

In this study, we assumed that both phantom lungs would have identical values of their various properties, such as density, coating thickness, and skin thickness. These, and other properties, may vary between the right and left lungs of a particular phantom lung set. This study did not consider the situation where the two phantom lungs were different. This would be an interesting topic for further study.

12.0 References

Berger MJ, JH Hubbell, SM Seltzer, J Chang, JS Coursey, R Sunumar and DS Zucker. 2005. XCOM: Photon Cross Section Database (version 1.3). [Online] Available: http://physics.nist.gov/xcom [2007, January 2]. National Institute of Standards and Technology, Gaithersburg, MD.

Blanchard BA. 2005. Email of elemental compositions for LN300 and LN450 lung materials made by Gammex RMI, Inc. Email dated 25-Aug-2005.

Dimbylow PJ. 1977. FDTD Calculations of the Whole-Body Averaged SAR in an Anatomically Realistic Voxel Model of the Human Body from 1 MHz to 1 GHz. Phys. Med. Biol. 42:479-490.

DOE – U.S. Department of Energy. 1998. *The Department of Energy Laboratory Accreditation Program for Radiobioassay*. DOE-STD-1112-98, U.S. Department of Energy, Washington, D.C.

Fry FA and TJ Summerling. 1982. The Design and Construction of a Realistic Thorax Phantom for in Vivo Measurements of Low-Energy Photon Emitters. Phys. Med. Biol. 27:1367-1379.

Griffith RV, PN Dean, AL Anderson, and JC Fisher. 1979. *A Tissue-Equivalent Torso Phantom For Intercalibration of in-Vivo Transuranic-Nuclide Counting Facilities*. p 493-504 of the Proceedings of the IAEA- International Symposium on Advances in Radiation Protection Monitoring, Stockholm, June 26-30, 1978. IAEA-SM-229/56.

HPS – Health Physics Society. 1996. *Performance Criteria for Radiobioassay*. ANSI/HPS N13.30-1996. Health Physics Society, McLean VA.

Hendricks JS, GW McKinney, LS Walters, TL Roberts, HW Egdorf, JP Finch, HR Trellue, EJ Pitcher, DR Mayo, MT Swinhoe, SJ Tobin, FK Gallmeier, J-C David, WB Hamilton, and J Lebenhaft. 2004. *MCNPX, Version 2.5.e.* LA-UR-04-0569, Los Alamos National Laboratory, Los Alamos NM.

ISO – International Organization for Standardization. 2001. *Radiation Protection – Performance Criteria for Radiobioassay – Part 1: General Principles*. ISO/FDIS 12790-1:2001(E). International Organization for Standardization, Geneva, Switzerland.

ICRP – International Commission on Radiological Protection. 2002. Basic Anatomical and Physiological Data for Use in Radiological Protection: Reference Values, ICRP Publication 89. Annals of the ICRP 32:1-277.

ICRU – International Commission on Radiation Units and Measurements. 1984. *Stopping Powers for Electrons and Positrons*. ICRU Report 37. International Commission on Radiation Units and Measurements. Bethesda MD.

ICRU – International Commission on Radiation Units and Measurements. 1989. *Tissue Substitutes in Radiation Dosimetry and Measurement*. ICRU Report 44. International Commission on Radiation Units and Measurements. Bethesda MD.

ICRU – International Commission on Radiation Units and Measurements. 1992a. *Phantoms and Computational Models in Therapy, Diagnosis and Protection.* ICRU Report 48. International Commission on Radiation Units and Measurements. Bethesda MD.

ICRU – International Commission on Radiation Units and Measurements. 1992b. *Photon, Electron, Proton and Neutron Interaction Data for Body Tissues*. ICRU Report 46. International Commission on Radiation Units and Measurements. Bethesda MD.

Johns HE and JR Cunningham. 1977. *The Physics of Radiology, Third Edition, Fourth Printing*. Charles C. Thomas. Springfield, IL.

Kinase, S., M Kimura, H Noguchi and S Yokoyama. 2005. *Development of Lung and Soft Tissue Substitutes for Photons*. Radiat. Prot. Dosim. 115(1-4):248-288

Spitz, H, S Glover, N Lui, B Smith D Hickman, D Kruchten and L Anderson. 1994. Measurement of the Attenuation Coefficient for Livermore Thoracic Phantom Lungs Fabricated Using Contemporary Materials. Health Phys. 67:39-46.

Taylor FY. 1997. *History of the Lawrence Livermore National Laboratory Torso Phantom*. Master of Science Thesis, San Jose State University. Available from UMI Dissertation Services, Ann Arbor, MI.

Traub RJ, PC Olsen and JC McDonald. 2006. *The Radiological Properties of a Novel Lung Tissue Substitute*. Radiat. Prot. Dosim. 121(2):202-207.

Pacific Northwest
NATIONAL LABORATORY

U.S. DEPARTMENT OF
ENERGY

902 Battelle Boulevard
P.O. Box 999
Richland, WA 99352
1-888-375-PNNL (7665)
www.pnl.gov